JACS
JOURNAL OF THE AMERICAN CHEMICAL SOCIETY

ARTICLE

pubs.acs.org/JACS

Diarylethene-Containing Cyclometalated Platinum(II) Complexes: Tunable Photochromism via Metal Coordination and Rational Ligand Design

Jacky Chi-Hung Chan,[†,‡] Wai Han Lam,[†,‡] Hok-Lai Wong,[†,‡] Nianyong Zhu,[‡] Wing-Tak Wong,[‡] and Vivian Wing-Wah Yam*[,†,‡]

[†]Institute of Molecular Functional Materials and [‡]Department of Chemistry, The University of Hong Kong, Pokfulam Road, Hong Kong, P.R. China

Supporting Information

ABSTRACT: The synthesis, characterization, electrochemistry, photophysics and photochromic behavior of a new class of cyclometalated platinum(II) complexes [Pt(C^N)(O^O)] (**1a**−**5a** and **1b**−**5b**), where C^N is a cyclometalating 2-(2′-thienyl)pyridyl (thpy) or 2-(2′-thienothienyl)pyridyl (tthpy) ligand containing the photochromic dithienylethene (DTE) unit and O^O is a β-diketonato ligand of acetylacetonato (acac) or hexafluoroacetylacetonato (hfac), have been reported. The X-ray crystal structures of five of the complexes have also been determined. The electrochemical studies reveal that the first quasi-reversible reduction couple, and hence the nature of lowest unoccupied molecular orbital (LUMO) of the complexes, is sensitive to the nature of the ancillary O^O ligands. Upon photoexcitation, complexes **1a**−**3a** and **1b**−**3b** exhibit drastic color changes, ascribed to the reversible photochromic behavior, which is found to be sensitive to the substituents on the pyridyl ring and the extent of π-conjugation of the C^N ligand as well as the nature of the ancillary ligand. The thermal bleaching kinetics of complex **1a** has been studied in toluene at various temperatures, and the activation barrier for the thermal cycloreversion of the complex has been determined. Density functional theory (DFT) calculations have been performed to provide an insight into the electrochemical, photophysical and photochromic properties.

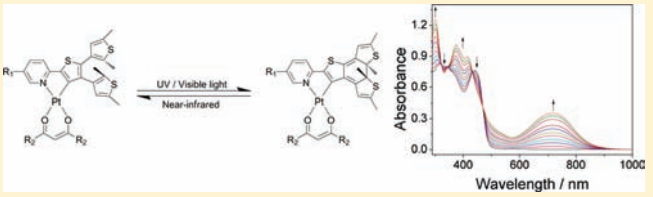

INTRODUCTION

The research on photochromic diarylethene compounds has received much attention in the past two decades because of their excellent thermal reversibility, fatigue resistance, distinguishable absorption spectra of the open form and the close form and possible future applications including optical memory storage systems and photoswitchable molecular devices.[1] Recently, various researchers have shown that the coordination of photochromic derivatives, such as azo,[2] stilbene,[3] diarylethene,[4−6] and spirooxazine,[7] to different metal centers can enrich the photochromic and photophysical behaviors, such as enhancement of the stability of the photochromic system by providing a triplet sensitizing pathway for the photochromic reaction. With regard to the diarylethene system that has attracted most attention, Yam and co-workers in 2004 first reported the functionalization of 1,10-phenanthroline with the diarylethene moiety to serve as a ligand for metal coordination,[6a] which is different from earlier studies,[4,5] in which the diarylethene unit was connected as a pendant to a ligating group. Yam and co-workers further tuned the photophysical and photochromic properties by coordination of the photochromic ligand to various metal centers, for instance, Re,[6a] Pt,[6g] and Zn.[6h] Very recently, various versatile photochromic ligands, such as *N*-heterocyclic carbenes,[6d,k,l] pyridylimidazole,[6m] and β-diketonate,[6i] have been prepared and incorporated into Au(I),[6d] Pd(II),[6d] Ag(I),[6d] Re(I),[6m] Pt(II),[6j] and B(III)[6i] centers to demonstrate the possibility of tunable photochromism.

On the other hand, cyclometalated platinum(II) complexes have been widely investigated as luminophores for efficient organic light-emitting diodes (OLEDs)[8,9] because the presence of heavy metal results in the strong spin-orbit coupling and efficient intersystem crossing between singlet and triplet states, which gives rise to higher triplet emission quantum yields.[10] It is interesting to note that there are no examples of functionalized cyclometalated platinum(II) complexes that show photochromic properties despite very few reports of examples of photochromic cyclometalated complexes of other metal centers.[5b,11] With our recent interest in the design, synthesis and tunable photochromic behaviors of various diarylethene-containing ligands and their metal complexes,[3c,f,6,7a,7d] we herein report the synthesis, characterization, photophysics, photochromic and eletrochemical properties of a new class of photochromic cyclometalated platinum(II) complexes, [Pt(C^N)(O^O)], where C^N is a cyclometalating 2-(2′-thienyl)pyridyl (thpy) or 2-(2′thienothienyl)pyridyl (tthpy) ligand containing the dithienylethene

Received: April 29, 2011
Published: July 22, 2011

Chart 1

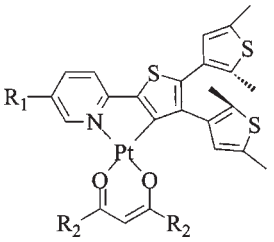

1a: $R_1 = H$ $R_2 = CH_3$
2a: $R_1 = CF_3$ $R_2 = CH_3$
3a: $R_1 = CH_3$ $R_2 = CH_3$
1b: $R_1 = H$ $R_2 = CF_3$
2b: $R_1 = CF_3$ $R_2 = CF_3$
3b: $R_1 = CH_3$ $R_2 = CF_3$

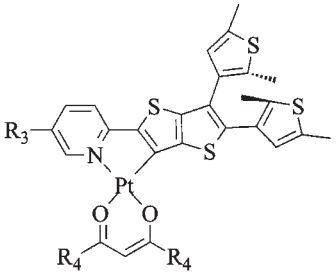

4a: $R_3 = H$ $R_4 = CH_3$
5a: $R_3 = CF_3$ $R_4 = CH_3$
4b: $R_3 = H$ $R_4 = CF_3$
5b: $R_3 = CF_3$ $R_4 = CF_3$

Table 1. Crystal and Structure Determination Data of Complexes 1a−3a, 1b and 4b

complex	1a	2a	3a	1b	4b
empirical formula	$C_{26}H_{25}NO_2PtS_3$	$C_{27}H_{24}F_3NO_2PtS_3$	$C_{27}H_{27}NO_2PtS_3$	$C_{26}H_{19}F_6NO_2PtS_3$	$C_{28}H_{19}F_6NO_2PtS_4$
formula weight	674.74	742.76	688.77	782.69	838.78
temp, K	301(2)	306(2)	301(2)	297(2)	305(2)
wavelength, Å	0.71073	0.71073	0.71073	0.71073	0.71073
crystal system	monoclinic	monoclinic	triclinic	orthorhombic	triclinic
space group	$P2_1/c$	$C2/c$ (No.15)	$P\bar{1}$ (No.2)	$Pbca$ (No.61)	$P\bar{1}$ (No.2)
a, Å	15.3344(8)	23.202(4)	8.4120(7)	24.4562(12)	7.0412(9)
b, Å	11.4973(6)	15.922(3)	9.6060(7)	7.1073(3)	12.5626(16)
c, Å	14.4707(8)	15.283(3)	16.498(1)	32.0980(15)	18.034(2)
α, deg	90	90	90.58(1)	90	96.176(2)
β, deg	97.947(10)	107.969(3)	92.95(1)	90	100.995(2)
γ, deg	90	90	91.31(1)	90	105.429(2)
volume, Å^3	2526.7(2)	5370.5(17)	1330.94(18)	5579.2(4)	1488.2(3)
Z	4	8	2	8	2
density (calcd), g/cm^3	1.774	1.837	1.719	1.864	1.872
crystal size	0.45 mm ×0.28 mm ×0.14 mm	0.06 mm ×0.20 mm ×0.27 mm	0.43 mm ×0.26 mm ×0.10 mm	0.10 mm ×0.29 mm ×0.35 mm	0.06 mm ×0.08 mm ×0.52 mm
index ranges	$-18 \le h \le 18$, $-12 \le k \le 14$, $-17 \le l \le 17$	$-25 \le h \le 27$, $-18 \le k \le 18$, $-18 \le l \le 12$	$-10 \le h \le 8$, $-11 \le k \le 11$, $-20 \le l \le 20$	$-31 \le h \le 31$, $-9 \le k \le 7$, $-41 \le l \le 41$	$-8 \le h \le 7$, $-14 \le k \le 14$, $-21 \le l \le 21$
reflections collected	15543	14506	8926	39893	8331
independent reflections	4790 [R(int) = 0161]	4740 [R(int) = 0.0225]	4930 [R(int) = 0.0175]	6385 [R(int) = 0.0440]	5148 [R(int) = 0269]
GOF on F^2	1.046	1.015	1.011	1.082	1.030
final R indices [$I > 2\sigma$ (I)]	$R_1 = 0.0192$ $wR_2 = 0.0484$	$R_1 = 0.0224$ $wR_2 = 0.0535$	$R_1 = 0.0189$ $wR_2 = 0.0472$	$R_1 = 0.0365$ $wR_2 = 0.0691$	$R_1 = 0.0325$ $wR_2 = 0.0892$
largest diff. peak and hole, e·Å^{-3}	1.216 and −0.656	0.888 and −0.540	0.721 and −0.727	0.932 and −2.540	2.391 and −1.304

(DTE) unit and O^O is a β-diketonate ligand of acetylacetonate (acac) or hexafluoroacetylacetonate (hfac) (Chart 1). Insights into the electronic structures of the complexes and the nature of their excited states have also been provided by DFT calculations.

RESULTS AND DISCUSSION

Synthesis and Characterization. Scheme S1 in Supporting Information (SI) summarizes the synthetic routes to the acac (**1a**−**5a**) and hfac (**1b**−**5b**) complexes in this study. 2,3-Bis(2,5-dimethylthiophen-3-yl)thieno[3,2-*b*]thiophene and 2,3-bis(2,5-dimethylthiophene-3-yl)thiophene were prepared by the reported procedure[6j] and were used as building blocks to synthesize the desired cyclometalating ligands, thpy-DTE and tthpy-DTE, respectively, via iridium-catalyzed C−H borylation[12] in the presence of bis-pinacolatodiboron and subsequent Suzuki cross-coupling reaction[13] with different bromopyridines. The target platinum(II) complexes **1a**−**5a** and **1b**−**5b** were prepared in two steps by modification of a literature procedure,[9e] in which the ligands were reacted with potassium tetrachloroplatinate(II) in aqueous 2-ethoxyethanol solution to yield a cyclometalated platinum(II) precursor, [Pt(C^N)(HC^N)Cl], followed by subsequent reaction between the precursor and Na(acac) or Na(hfac)

Table 2. Selected Bond Lengths [Å] and Angles [deg] for Complexes 1a−3a, 1b and 4b with Estimated Standard Deviations (esds) Given in Parentheses

1a		2a		3a		1b		4b	
Pt(1)−O(1)	2.065(2)	Pt(1)−O(2)	2.064(2)	Pt(1)−O(1)	2.083(2)	Pt(1)−O(1)	2.082(4)	Pt(1)−O(1)	2.087(3)
Pt(1)−O(2)	1.989(2)	Pt(1)−O(1)	1.999(2)	Pt(1)−O(2)	1.990(2)	Pt(1)−O(2)	2.012(3)	Pt(1)−O(2)	2.011(4)
Pt(1)−C(7)	1.979(3)	Pt(1)−C(7)	1.985(3)	Pt(1)−C(7)	1.986(3)	Pt(1)−C(7)	1.989(5)	Pt(1)−C(7)	1.961(5)
Pt(1)−N(1)	1.998(2)	Pt(1)−N(1)	2.006(3)	Pt(1)−N(1)	1.997(2)	Pt(1)−N(1)	1.989(4)	Pt(1)−N(1)	1.994(4)
C(7)−Pt(1)−N(1)	81.58(10)	C(7)−Pt(1)−N(1)	81.69(12)	C(7)−Pt(1)−N(1)	81.64(11)	C(7)−Pt(1)−N(1)	82.17(17)	C(7)−Pt(1)−N(1)	81.4(2)
O(2)−Pt(1)−O(1)	92.35(8)	O(1)−Pt(1)−O(2)	92.43(10)	O(2)−Pt(1)−O(1)	91.33(9)	O(2)−Pt(1)−O(1)	90.85(15)	O(2)−Pt(1)−O(1)	92.20(15)
N(1)−Pt(1)−O(1)	91.05(9)	N(1)−Pt(1)−O(2)	89.92(11)	N(1)−Pt(1)−O(1)	92.37(10)	N(1)−Pt(1)−O(1)	89.70(16)	N(1)−Pt(1)−O(1)	93.48(17)
C(7)−Pt(1)−O(2)	94.84(9)	C(7)−Pt(1)−O(1)	95.99(12)	C(7)−Pt(1)−O(2)	94.66(11)	C(7)−Pt(1)−O(2)	97.29(16)	C(7)−Pt(1)−O(2)	92.88(18)
O(2)−Pt(1)−N(1)	174.96(9)	O(1)−Pt(1)−N(1)	177.43(10)	O(2)−Pt(1)−N(1)	176.28(9)	O(2)−Pt(1)−N(1)	177.85(16)	O(2)−Pt(1)−N(1)	174.08(15)
C(7)−Pt(1)−O(1)	172.22(10)	C(7)−Pt(1)−O(2)	171.43(12)	C(7)−Pt(1)−O(1)	174.00(10)	C(7)−Pt(1)−O(1)	171.85(17)	C(7)−Pt(1)−O(1)	174.82(16)

in dichloromethane to afford the crude products as orange to red solids. Recrystallization by layering of methanol onto a concentrated dichloromethane solution of the complexes gave the desired complexes as orange to red crystals. The identities of complexes **1a**−**5a** and **1b**−**5b** have been confirmed by ^{1}H NMR spectroscopy, ^{19}F NMR spectroscopy for the hfac complexes as well, FAB mass spectroscopy and satisfactory elemental analyses. The crystal structures of complexes **1a**−**3a**, **1b** and **4b** have also been determined by X-ray crystallography.

X-ray Crystal Structures. Single crystals of **1a**−**3a**, **1b** and **4b** were obtained by layering of methanol onto a concentrated dichloromethane solution of the respective complexes, and their structures were determined by X-ray crystallography. Crystal structure determination data are summarized in Table 1. The selected bond distances, bond angles, and intermolecular parameters are tabulated in Tables 2 and 3, respectively. The perspective views of the crystal structures of complexes **1a** and **4b** are depicted in Figure 1, whereas those of **2a**, **3a** and **1b** are depicted in Figure S1 (SI).

In each case, the platinum(II) center adopts a distorted square-planar geometry with the C−Pt−N and O−Pt−O angles in the range of the 81.40−82.17° and 90.85−92.43°, respectively. The C−Pt−N and O−Pt−O chelate planes are not perfectly coplanar in **1a**, **2a**, **1b** and **4b** with the interplanar angle between the two chelate rings in the range of 3.00−8.52°. The Pt−C (1.961−1.989 Å) and Pt−N (1.989−2.006 Å) distances are comparable to the literature reported values in related systems.[9b,d,f,14,15] The Pt−O bond (2.065−2.087 Å) *trans* to the thienyl carbon are found to be longer than the Pt−O bond (1.989−2.012 Å) *trans* to the pyridyl nitrogen, which is attributed to the stronger *trans* influence of the metalated carbon. For complexes **1a**, **1b** and **4b**, the two thiophene rings are arranged in an antiparallel configuration, while they are in parallel configuration for complexes **2a** and **3a**. The interplanar angles between the two peripheral thiophene rings and the Pt(thpy/tthpy) core of the complexes are in the range of 40.49−74.87°, indicating that the two thiophene rings are slightly π-conjugated to the thpy/tthpy core.

In the solid state crystal structure packing, each complex packs together in pairs, as exemplified by the crystal packing diagram of **1b** and **4b** in Figure S2 (SI). The plane-to-plane separation of these complexes are found in the range of 3.31−3.88 Å and $\pi-\pi$ stacking interactions are present in complexes **3a** and **4b**, as indicated by the plane-to-plane separation between two molecules of 3.39 Å and 3.31 Å, respectively.[9b,d,f,16] On the other hand, only complex **4b** is found to have short Pt···Pt distances of 3.58 Å, suggesting that weak Pt···Pt interaction is present in its crystal structure.

Electrochemical Studies. Most complexes show two irreversible oxidation waves in their cyclic voltammograms in dichloromethane (0.1 mol dm^{-3} ^{n}Bu$_4$NPF$_6$). The electrochemical data for the complexes are tabulated in Table 4. The representative cyclic voltammograms of complexes **2a** and **2b** are depicted in Figures S3 and S4 in the SI, respectively. The first irreversible oxidation wave is in the range of +1.01 to +1.38 V vs SCE. Interestingly, the cyclic voltammograms of the reduction for the hfac analogues (**1b**−**5b**) are quite different from that of the acac complexes (**1a**−**5a**). Complexes **1b**−**5b** show two reduction waves, a quasi-reversible couple at −1.07 to −1.24 V vs SCE and an irreversible reduction wave at −1.78 to −2.06 V vs SCE. For the acac complexes, only one irreversible reduction wave was

Table 3. Selected Intermolecular Parameters of Complexes 1a−3a, 1b and 4b

complex	1a	2a	3a	1b	4b
shortest Pt···Pt distances/Å	5.13	3.69	4.88	4.94	3.58
interplanar separations between two molecules/Å	3.88	3.63	3.39	3.53	3.31
interplanar angles between [Pt(N^C)(O^O)]/deg	0.00	1.73	0.00	1.64	0.00
interplanar angle between two chelate rings/deg	8.52	3.72	1.41	3.42	3.00
interplanar angles between dimethylthiophene rings and the thinothiophene core/deg	74.87 and 63.30	40.49 and 64.56	52.10 and 63.80	55.40 and 50.53	47.57 and 47.35

observed for **2a** (−1.90 V), **4a** (−2.02 V) and **5a** (−1.60 V), while no reduction wave was observed for **1a** and **3a** even upon scanning to −2.10 V vs SCE.

As shown in Table 4, the first oxidation wave is shifted to less positive potential upon going from the thienylpyridyl complexes (**1** and **2**) to the thieno[3,2-*b*]thienylpyridyl complexes (**4** and **5**). In addition, the ease of oxidation shows a trend of **3** > **1** > **2**, in line with the electron-donating ability of the substituents on the pyridyl unit CH_3 > H > CF_3. In view of the observed change of the potentials for oxidation upon varying the electronic properties of the C^N ligand, the oxidation is tentatively assigned as C^N ligand-centered oxidation, mixed with some metal-centered contribution. On the other hand, the first reduction potentials are strongly affected by the nature of the ancillary β-diketonate ligand, with a significant positive shift of ∼0.53−0.91 mV observed for the hfac complexes **2b**, **4b**, and **5b** with respect to their acac analogues, suggesting that the first reduction of the two analogues may have different origins. Since the first reduction potential for the hfac complexes is insensitive to the nature of the C^N ligand while a substantial change of the reduction potential is observed for the acac complexes upon varying the nature of the C^N ligand, it is suggested that the first reduction couple for the hfac and acac complexes arise from the O^O ligand-based and C^N ligand-based reductions, respectively. The electrochemical behavior has been further supported by the DFT calculations (vide infra).

Electronic Absorption and Emission Properties. All complexes are found to dissolve in benzene to give a clear yellow solution. In general, the electronic absorption spectra of **1a**−**5a** and **1b**−**5b** in benzene at 298 K show an intense absorption band at ∼296−394 nm and a moderately intense band at ∼416−485 nm. For complexes **1b**, **4b** and **5b**, in addition to these absorption bands, a very weak absorption tail at ∼473−520 nm has been observed (Figure S5, SI). The photophysical data of **1a**−**5a** and **1b**−**5b** are summarized in Table 4, and the corresponding electronic absorption spectra of **1a**−**3a** are depicted in Figure 2. The high-energy intense absorption band is probably assigned to an admixture of intraligand (IL) $\pi-\pi^*$ transition of C^N ligand, ligand-to-ligand charge transfer transition (LLCT) from π orbitals of the C^N ligand to π^* orbitals of the O^O ligands and metal-to-ligand charge transfer (MLCT) transitions. For the low-energy absorption band, although it is only slightly perturbed with the electron-donating CH_3 group on the pyridyl ring (**1** vs **3**), it is red-shifted upon going from the nonsubstituted C^N complexes (**1** and **4**) to the CF_3-substituted complexes (**2** and **5**) as well as going from the thienylpyridyl complexes (**1** and **2**) to the thieno[3,2-*b*]thienylpyridyl complexes (**4** and **5**). Since the low-energy absorption band is sensitive to substituents on the pyridyl ring and the extent of π-conjugation of the C^N ligand, it is assigned to the IL $\pi-\pi^*$ transition of the C^N ligand with some mixing of MLCT transition. The absorption band at 438 nm in benzene is slightly shifted to higher energies as the polarity of the solvent increases as indicated in Figure S6 (SI) and the dependence of the absorption energy on the Dimroth's solvent parameter in Figure S7 (SI), which is in agreement with the assignment of the low-energy absorption band. This has further been supported by the TDDFT calculations.

Upon excitation at $\lambda \geq 300$ nm, solid samples and benzene solutions of the platinum(II) complexes exhibit intense red luminescence at both room temperature and 77 K. The emission data for the complexes are tabulated in Table 4. Upon excitation at room temperature, complexes **1a**−**5a** and **1b**−**5b** in benzene solution display luminescence at ∼647−717 nm, with lifetimes in the microsecond range. The large Stokes shifts together with the long-lived emission are suggestive of an origin of triplet parentage. The complexes show vibrational progressional spacings of ∼1000 cm^{-1}, typical of vibrational modes of the heterocyclic ligands. The energies of these emissions are found to be sensitive to the nature of the substituents on the pyridyl unit and the extent of the π-conjugation of the C^N ligand. However, the complexes with hfac ligand show a slight bathochromic shift compared to the complexes with acac ligand. With reference to previous work on [Pt(C^N)(O^O)],[9e,17] the emission is believed to be mainly derived from the ^{3}IL $\pi-\pi^*$ origin of the C^N ligand. Parallel to the electronic absorption study, the emission band of the CF_3-substituted complexes (**2** and **5**) occurs at lower energy than that of nonsubstituted complexes (**1** and **4**). The introduction of the weak σ-donating methyl group at the 5-position of the pyridyl ring leads to a slight change in the emission band (**1** vs **3**). The corresponding normalized corrected emission spectra of the open form of **1a**−**3a** are depicted in Figure 3 and the excitation spectra are shown in Figure S8 (SI), which closely resemble that of the UV−vis absorption spectra (Figure 2). Although the increase in the extent of π-conjugation upon introduction of a fused thiophene unit on the thienyl moeity in **4** and **5** is anticipated to lower the $\pi-\pi^*$ energy separation of the C^N ligand relative to **1** and **2**, respectively, as observed in the electronic absorption study, only a very small to negligible shift of this vibronic-structured emission band was observed in **4** and **5**.

For emission studies in low-temperature glasses, all the complexes show vibronic-structured emission bands at approximately 597−767 nm. The emissions in 77 K glass show a blue shift relative to the emissions at room temperature.

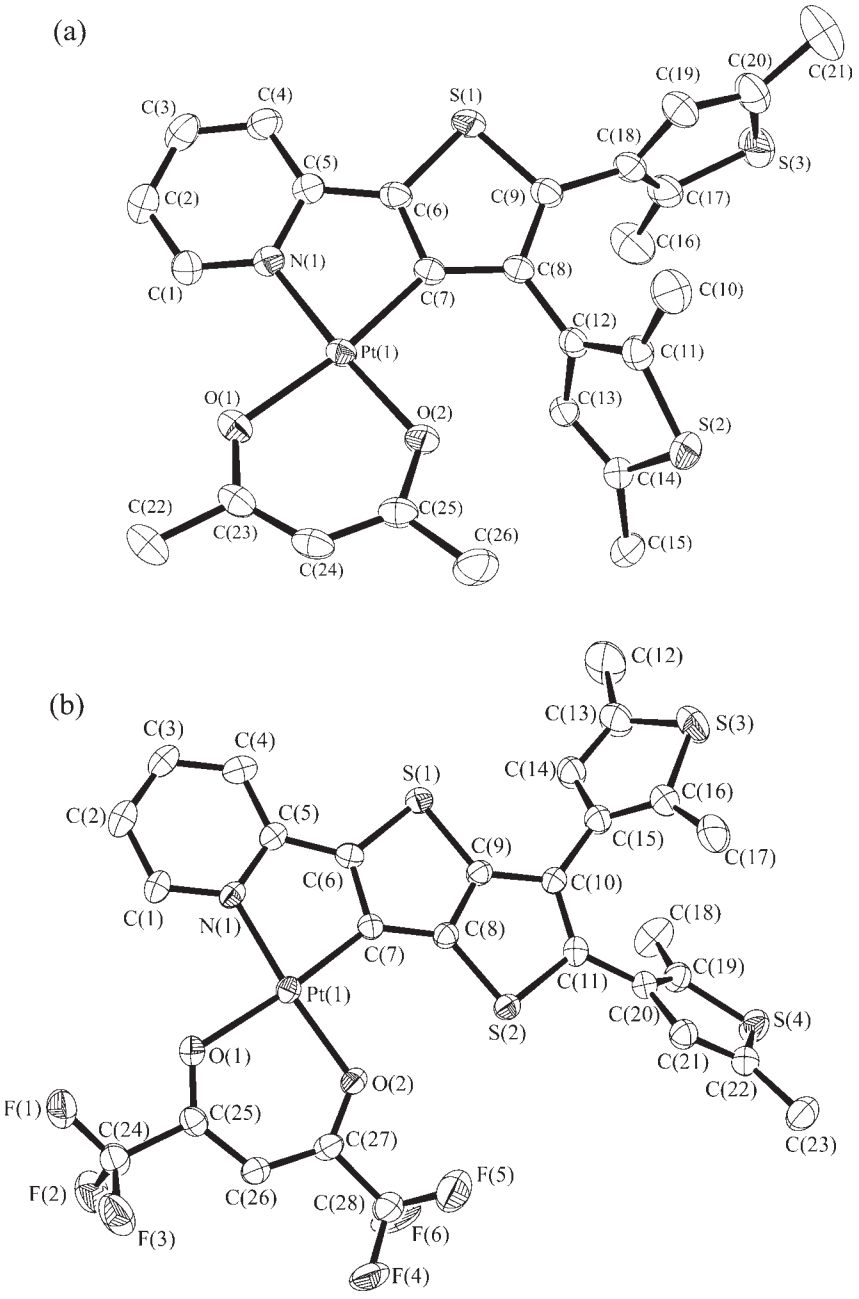

Figure 1. Perspective views of complex (a) **1a** and (b) **4b** with atomic numbering scheme. Hydrogen atoms have been omitted for clarity. Thermal ellipsoids were shown at the 30% probability level.

The luminescence quantum yields of these complexes were found to vary from 0.001 to 0.141. As depicted in Table 4, the hfac complexes exhibit lower phosphorescence quantum yields when compared with the corresponding acac complexes. In addition to the triplet emission, singlet emissions have also been observed in the range of 468−514 nm in **1**−**5**. The singlet emission energies in **1**−**5** follow essentially the same trend as the low-energy absorption band in the electronic absorption spectra, indicating that the emission is originated from the ^{1}IL $\pi-\pi^*$ excited state of the C^N ligand. The ratio between the singlet and the triplet emission intensities is larger in the hfac complexes (0.036−0.874) than that of the acac complexes (0.010−0.055). The normalized corrected emission spectra of **4a** and **4b** are shown in Figure S9 (SI). The lower phosphorescence quantum yields observed for hfac complexes are probably due to the less effective intersystem crossing process for the hfac complexes.

Photochromic Properties. Upon IL photoexcitation at λ = 330 nm or IL/MLCT excitation at λ = 440 nm, complexes **1a**−**3a** and **1b**−**3b** undergo photocyclization and the solutions turn green, with the emergence of low-energy absorption bands from 638 to 719 nm with molar extinction coefficients in the order of 10^3 dm^3 mol^{-1} cm^{-1}. The UV−vis absorption spectral changes of **1a** in benzene are shown in Figure 4. The significant bathochromic shift in absorption maxima of the closed forms relative to their open forms is mainly due to the extended π-conjugation across the 8a,8b-dimethyl-1,8-thia-*as*-indacene moiety. However, upon photoexcitation of complexes **4a**, **5a**, **4b** and **5b**, no significant

dx.doi.org/10.1021/ja203946g |*J. Am. Chem. Soc.* 2011, 133, 12690–12705

Table 4. Photophysical and Electrochemical Data of Complexes 1a−5a and 1b−5b

		absorption[a]	emission			oxidation[h]	reduction[h]
complex	configuration	λ_{abs}/nm (ε/dm^3 mol^{-1} cm^{-1})	medium (T/K)	λ_{em}/nm (τ_o/μs)[d]	ϕ_{lum}[e,g]	$E_{1/2}$[i]/V vs SCE (ΔE_p/mV)[c] [E_{pa}[k]/V vs SCE]	$E_{1/2}$[i]/V vs SCE (ΔE_p/mV)[c,j] [E_{pc}[l]/V vs SCE]
[Pt(thpy-DTE)(acac)] (**1a**)	open	336 (22480), 374 sh (14960), 422 (10080), 438 (10080)	benzene (298)	648, 694 (9.56)	0.020	[+1.23, +1.61][g]	−[m]
			solid (298)	599, 639, 689 sh (0.14)			
			solid (77)	607, 641, 694 sh (0.14)			
			glass[f] (77)	597, 651, 705 sh (30.17)			
	close	348 sh (23580), 364 (25070), 390 sh (16130), 456 (7460), 638 (9290)	−	−	−	−	−
[Pt(CF$_3$-thpy-DTE)(acac)] (**2a**)	open	299 (10060), 349 (11650), 364 sh (10300), 394 (8730), 442 (6420), 462 (6780)	benzene (298)	657, 704 (14.91)	0.063	[+1.24, +1.49][g]	[−1.90]
			solid (298)	651, 684 (1.26)			
			solid (77)	640, 692 (1.14)			
			glass[f] (77)	609, 663 (190.2)			
	close	299 (15850), 378 (13040), 411 sh (8380), 461 sh (5360), 695 (4600)	−	−	−	−	−
[Pt(Me-thpy-DTE)(acac)] (**3a**)	open	336 (21660), 368 sh (13890), 424 (9010), 438 (8970)	benzene (298)	650, 695 (7.10)	0.019	[+1.01, +1.34]	−[m]
			solid (298)	619, 651 (0.14)			
			solid (77)	621, 676 (0.15)			
			glass[f] (77)	598, 653, 711 sh (20.48)			
	close	344 (21540), 358 sh (20270), 388 sh (12530), 448 sh (6500), 632 (5930)	−	−	−	−	−
[Pt(tthpy-DTE)-(acac)] (**4a**)	open	296 (12510), 346 (25850), 368 sh (17880), 440 (13240), 462 (13510)	benzene (298)	647, 690 (14.30)	0.044	[+1.12, +1.35]	[−2.02]
			solid (298)	641, 691, 760 (0.81)			
			solid (77)	649, 695, 762 (1.02)			
			glass[f] (77)	623, 678, 749 (32.80)			
	close	618[b]	−	−	−	−	−
[Pt(CF$_3$-tthpy-DTE)(acac)] (**5a**)	open	302 (13180), 357 (22340), 369 (22200), 388 sh (16210), 462 (14720), 485 (16560)	benzene (298)	656, 702 (22.36)	0.141	[+1.13, +1.36]	[−1.60]
			solid (298)	659, 710, 769 sh (1.07)			
			solid (77)	648, 686, 747 sh (0.94)			
			glass[f] (77)	620, 678, 746 (28.58)			
	close	646[b]	−	−	−	−	−
[Pt(thpy-DTE)(hfac)] (**1b**)	open	303 sh (12950), 320 (13710), 346 sh (11200), 416 (10820)	benzene (298)	651, 697 (6.27)	0.009	[+1.25, +1.76]	−1.23 (141), [−2.04]
			solid (298)	697 (0.22)			
			solid (77)	657, 725 (0.19)			
			glass[f] (77)	608, 657 (36.54)			
	close	294 (19160), 340 sh (13910), 364 (16820), 375 (16750), 393 sh (15330), 446 sh (5630), 654 (6350)	−	−	−	−	−

Table 4. Continued

		absorption[a]	emission				
complex	configuration	λ_{abs}/nm (ε/dm^3 mol^{-1} cm^{-1})	medium (T/K)	λ_{em}/nm (τ_o/μs)[d]	ϕ_{lum}[e,g]	oxidation[h] $E_{1/2}$[i]/V vs SCE (ΔE_p/mV)[c] [E_{pa}[k]/V vs SCE]	reduction[h] $E_{1/2}$[i]/V vs SCE (ΔE_p/mV)[c,j] [E_{pc}[l]/V vs SCE]
[Pt(CF_3-thpy-DTE)-(hfac)] (**2b**)	open	319 (11930), 338 sh (11630), 366 sh (10640), 441 (11030)	benzene (298)	663, 711 (12.18)	0.028	[+1.38, +1.79]	−1.18 (104), [−2.06]
			solid (298)	631, 667 (1.16)			
			solid (77)	660 (21.26)			
			glass[f] (77)	623, 666 (54.84)			
	close	300 (20040), 374(15860), 413 (14140), 464 sh (6310), 719 (6490)	–	–	–	–	–
[Pt(Me-thpy-DTE)-(hfac)] (**3b**)	open	320 (15410), 344 sh (12740), 416 (11010)	benzene (298)	655, 701 (4.42)	0.006	[+1.20]	−1.24 (98), [−1.78]
			solid (298)	620, 651 (0.22)			
			solid (77)	630, 674 (9.06)			
			glass[f] (77)	613, 660 (21.96)			
	close	290 (20150), 334 sh (15450), 356 (16290), 374 (16010), 390 sh (15140), 436 sh (6780), 642 (5210)	–	–	–	–	–
[Pt(tthpy-DTE)-(hfac)] (**4b**)	open	332 (17900), 358 (18240), 438 (15530), 456 (14290)	benzene (298)	659, 705 (8.82)	0.001	[+1.17]	−1.11 (98), [−1.92]
			solid (298)	645, 690, 762 (0.89)			
			solid (77)	629, 689, 762 (1.30)			
			glass[f] (77)	636, 692, 759 sh (27.96)			
	close	–[c]	–	–	–	–	–
[Pt(CF_3-tthpy-DTE) (hfac)] (**5b**)	open	343 (8110), 370 (8840), 460 (8830), 480 (8860)	benzene (298)	669, 717 (12.48)	0.037	[+1.25, +1.59]	−1.07 (73), [−1.84]
			solid (298)	656, 711, 782 sh (0.83)			
			solid (77)	653, 716, 784 sh (4.73)			
			glass[f] (77)	648, 707, 767 (48.22)			
	close	663[b]	–	–	–	–	–

[a] Data obtained in benzene at 298 K. [b] Conversion percentage was too low to be precisely measured by NMR spectroscopy to obtain extinction coefficients for the corresponding closed form. [c] The absorption wavelength of the closed form could not be precisely determined because no obvious UV−vis absorption spectral change was observed upon prolonged irradiation. [d] Emission maxima are corrected values. [e] Luminescence quantum yields are reported using a degassed aqueous solution of [Ru(bpy)$_3$]Cl$_2$ as standard at 298 K. [f] Butyronitrile. [g] Luminescence quantum yields of the triplet emission. [h] Working electrode, glassy carbon; scan rate, 100 mV s^{-1}. [i] $E_{1/2} = (E_{pa} + E_{pc})/2$; E_{pa} and E_{pc} are anodic and cathodic peak potentials, respectively. [j] $\Delta E_p = (E_{pa} - E_{pc})$. [k] E_{pa} is reported for irreversible oxidation wave. [l] E_{pc} is reported for irreversible reduction wave. [m] No reduction wave was observed.

color changes are observed in the solution, suggesting the occurrence of a relatively inefficient photocyclization process and only a weak absorption band is found to appear at 618−663 nm. Because of this, the extinction coefficients of the closed forms for these complexes could not be determined with certainty.

The lowest-energy absorption band of the closed form was found to be red-shifted upon going from the acac complexes to the hfac complexes (see Figure 5 for **2a** vs **2b**). Apart from the effect of the ancillary β-diketonate ligand on the Pt center, the absorption band is also found to be tunable by varying the substituents attached to the pyridyl ring (Figure 6). The introduction of the electron-withdrawing CF_3 group leads to a significant red shift in the lowest-energy absorption band of the closed form in complexes **2a** and **2b** when compared with that of the nonsubstituted analogues **1a** and **1b**. On the contrary, the introduction of the electron-donating methyl group leads to a blue shift of the lowest-energy absorption band of the closed form. Interestingly, the increase in the extent of π-conjugation in the thienylpyridine ligand of the complexes (**1** vs **4** and **2** vs **5**) results in a blue-shift of the lowest-energy absorption band. The calculations are in agreement with the observed trend in the low-energy absorption (vide infra).

Upon photoexcitation into the absorption band at about 600−800 nm in the closed form, the UV−vis absorption spectral

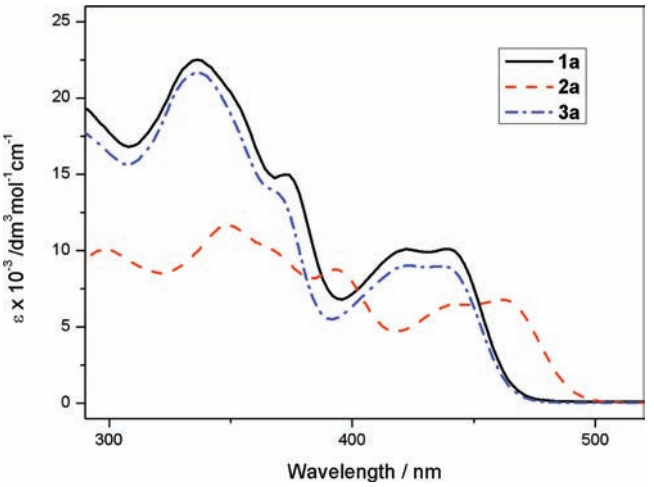

Figure 2. Electronic absorption spectra of the open forms of complexes **1a**−**3a** in benzene at 298 K.

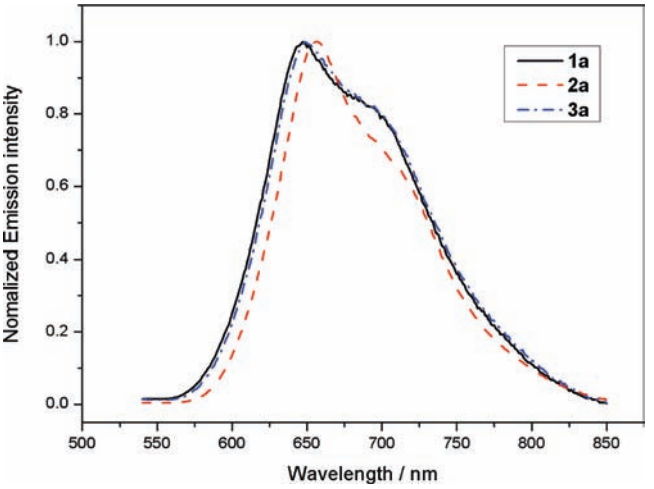

Figure 3. Normalized corrected emission spectra of the open forms of **1a**−**3a** in degassed benzene at 298 K with excitation at λ = 436 nm.

changes were reversed, resulting in photocycloreversion to regenerate the open form. The reversibility of the photochromic behavior has been studied on a representative sample of complex **1a**. As shown in Figure 7, the complex shows good reversibility in its photochromic behavior, with no apparent loss in its photochromic reactivities over at least five repeating cycles.

In these cyclometalated platinum complexes, the photocyclization quantum yields are in the range of <0.001 to 0.079 and the photocycloreversion quantum yields are in the range of 0.002−0.037, which are summarized in Table 5. It is found that the photocyclization quantum yield can be increased upon changing the ancillary ligand from hfac to acac, probably due to the less effective competing radiative decay processes in the acac complexes.

The photocyclization conversion from the open form to the closed form on 440 nm excitation for complexes **1a**−**3a** and **1b**−**3b** are found to be 33−79 % at the photostationary state, whereas the percentage conversion for complexes **4a**, **5a**, **4b** and **5b** at the photostationary state has been too low to be precisely measured. Our studies demonstrate that the nature of the

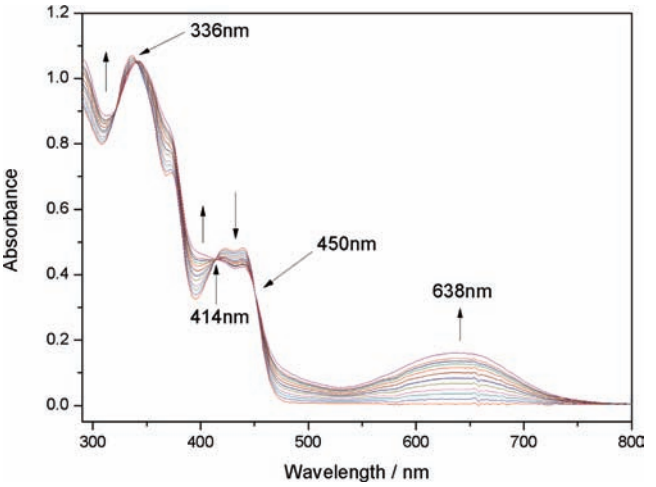

Figure 4. UV−Vis absorption spectral changes of **1a** in benzene upon excitation at λ = 440 nm at 298 K.

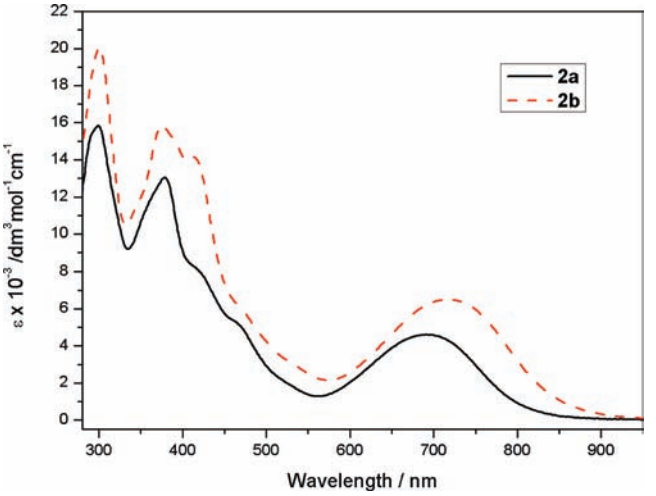

Figure 5. Electronic absorption spectra of closed form of complexes **2a** and **2b** in benzene at 298 K.

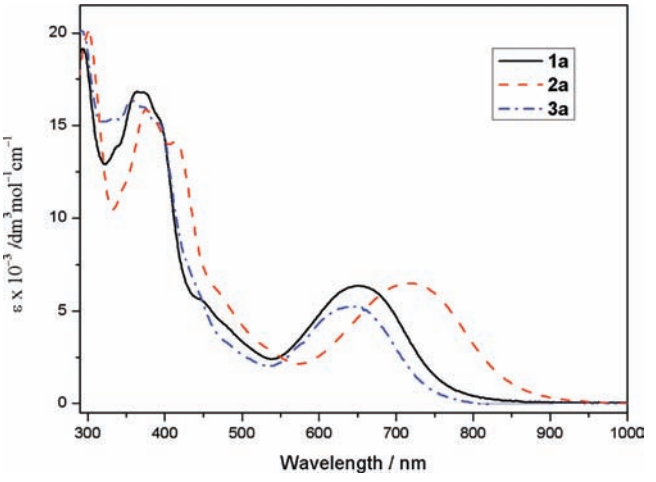

Figure 6. Electronic absorption spectra of closed form of complexes **1a**−**3a** in benzene at 298 K.

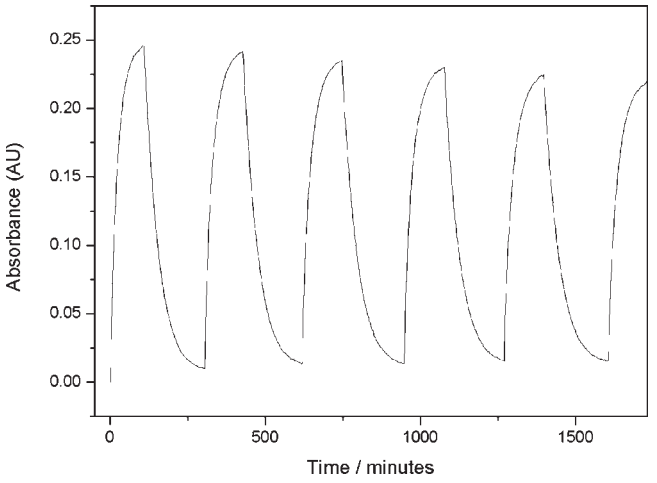

Figure 7. UV−Vis absorbance changes of complex **1a** at 638 nm on alternate excitation at 440 and 638 nm over five cycles in degassed benzene solution at 293 K.

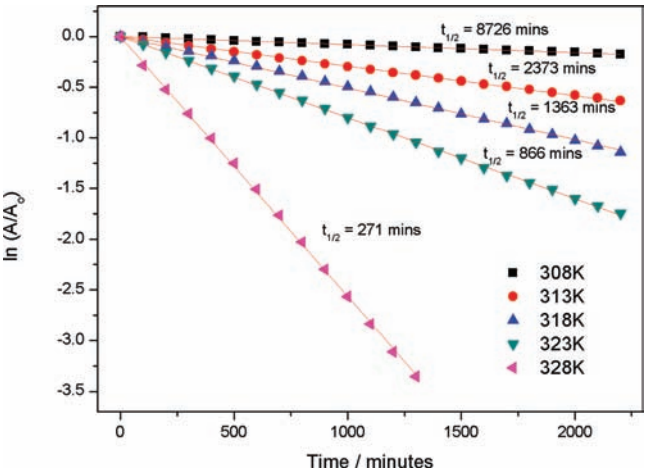

Figure 8. Plot of $\ln(A/A_o)$ versus time for the absorbance decay of complex **1a** at 638 nm at various temperatures in argon-flushed toluene solution; A denotes absorbance at time t and A_o denotes the initial absorbance; solid lines represent the theoretical linear fits.

Table 5. Photochemical Quantum Yields and the Percentage Conversion at Photostationary State (PSS) for Complexes 1a−5a and 1b−5b in Degassed Benzene Solution at 298 K

	photochemical quantum yield/ϕ^a		
complex	photocyclization	photocycloreversion	conversion at PSS (%)
[Pt(thpy-DTE)-(acac)] (**1a**)	0.079[b]	0.013[c]	36[b]
[Pt(CF$_3$-thpy-DTE)-(acac)] (**2a**)	0.0082[b]	0.016[c]	65[b]
[Pt(Me-thpy-DTE)-(acac)] (**3a**)	0.0049[b]	0.037[c]	33[b]
[Pt(tthpy-DTE)-(acac)] (**4a**)	−[d]	−[d]	<5[b,d]
[Pt(CF$_3$-tthpy-DTE)-(acac)] (**5a**)	−[d]	−[d]	<5[b,d]
[Pt(thpy-DTE)-(hfac)] (**1b**)	0.0057[b]	0.0025[c]	67[b]
[Pt(CF$_3$-thpy-DTE)-(hfac)] (**2b**)	0.0075[b]	0.0038[c]	79[b]
[Pt(Me-thpy-DTE)-(hfac)] (**3b**)	0.0007[b]	0.0018[c]	52[b]
[Pt(tthpy-DTE)-(hfac)] (**4b**)	−[d]	−[d]	<5[b,d]
[Pt(CF$_3$-tthpy-DTE)-(hfac)] (**5b**)	−[d]	−[d]	<5[b,d]

[a] Data obtained with an uncertainty of ±10%. [b] Data obtained using 440 nm as the excitation source. [c] Data obtained using 600 nm as the excitation source. [d] Conversion rate and percentage were too low to be precisely measured by NMR spectroscopy.

ancillary β-diketonate ligand and C^N ligand not only would affect the wavelength of the absorption band of the closed form but also the photocyclization conversion at the photostationary state.

A study of the thermal stability of the closed form has been performed on **1a** and the plots of $\ln(A/A_o)$ versus time for the absorbance decay of complex **1a** at 638 nm at various temperatures are shown in Figure 8. The complex undergoes slow thermal backward reactions even at 308 K and the half-life for the closed form is about 8726 min, which is determined by plotting $\ln(K)$ versus T^{-1} (Figure S10 in SI) using the Arrhenius equation. The activation energy of the thermal cycloreversion of **1a** has been found to be 133.7 kJ mol^{-1}, indicating that the complex has a sufficiently thermal-stable closed form.

Computational Studies. Density functional theory (DFT) and time-dependent (TD-DFT) calculations at the PBE0 level of theory have been performed to study the open and closed forms for **1a**−**5a** and **1b**−**5b** in order to gain further insights into the nature of absorption and emission origins of these complexes. Details of the optimized structures are given in the SI (Figure S11 and Table S1).

The spatial plots of selected TDDFT/CPCM frontier molecular orbitals (MOs) for the open and closed forms in **1a** and **1b**, and **4a** and **4b** are respectively shown in Figure 9 and Figure S12 (SI), and the percentage contributions of selected MOs and orbital energies for the two forms in all the complexes are listed in Tables S2 and S3 (SI). For the open forms in **1a**−**5a**, the HOMO of each is the π orbital of the thpy-DTE or tthpy-DTE ligands slightly mixed with the metal dπ orbital with the Pt−C orbital overlap being antibonding in character, while the LUMO is the π^* orbital mainly localized on the thpy/tthpy core. For **1b**−**5b**, the HOMO of each is similar to those in the acac analogues. Interestingly, unlike the LUMO in the acac analogues, the LUMO in the hfac analogues is the π^* orbital localized on the ancillary hfac ligands (Figure 9). This fact can be readily rationalized as a consequence of the electronegativity of the fluorine atoms, which induces a large stabilization of the π^* orbitals of the O^O ligand. The LUMO+1 of **1b**−**5b** is similar to the LUMO of the corresponding acac analogues, which is the π^* orbital of the thpy/tthpy core. The calculated HOMO and LUMO in **1a**−**5a** and **1b**−**5b** confirm the assignment of the first oxidation and reduction processes in the electrochemical study, respectively.

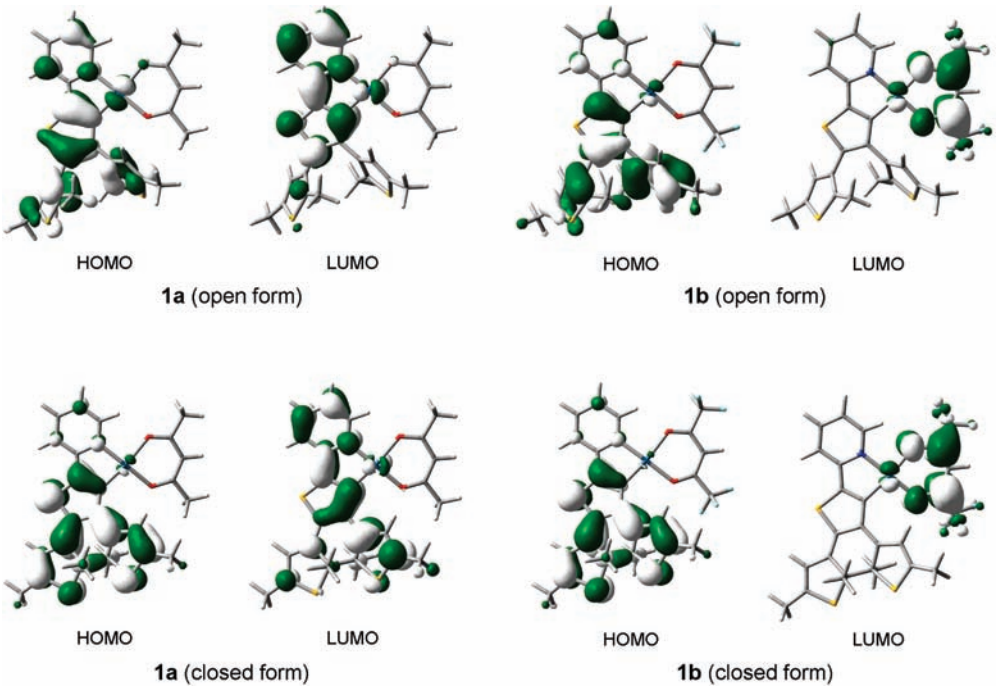

Figure 9. Spatial plots (isovalue = 0.03) of the HOMO and LUMO for the two forms in **1** obtained from the TDDFT/CPCM calculations.

For the closed forms in each complex, the HOMO is the π orbital localized on the condensed ring of the dithienylthiophene unit. On the other hand, the LUMO is predominantly the π^* orbital delocalized over the whole C^N ligand with the exception of **1b**, **3b** and **4b**, in which the LUMO is the π^* orbital of the hfac ligand. As shown in Table S3 (SI), a significant decrease in the HOMO−LUMO energy gap is found in the closed forms (2.09−2.42 eV) relative to the open forms (3.21−3.87 eV).

Selected singlet−singlet transitions of the open and closed forms in **1a**−**5a** and **1b**−**5b** are listed in the Table S4 and S5 (SI), respectively. For the open forms in **1a**−**5a**, the lowest-lying singlet−singlet transition computed at 406−446 nm is composed of HOMO → LUMO excitation and can be assigned as the IL π−π^* transition of the C^N ligand, with some mixing of MLCT [Pt(dπ) → π^*(C^N)] character. On the other hand, the first singlet−singlet transition for the open forms in **1b**−**5b**, which is computed to be relatively less intense and at lower energies (445−477 nm), is mainly contributed by the HOMO → LUMO excitation and can be assigned as LLCT transition from the π orbital of the C^N ligand to the π^* orbital of the ancillary O^O ligand. The IL/MLCT transition ($S_0 \rightarrow S_2$ for **2b**, **4b**, and **5b** and $S_0 \rightarrow S_3$ for **1b** and **3b**), which is similar to the first singlet−singlet transition in the acac complexes, is computed at 406−449 nm.

For the closed forms in **1a**−**5a**, the lowest-energy singlet−singlet transition (650−761 nm) can be assigned as the IL π−π^* transition from the π orbital localized on the condensed ring of the dithienylthiophene unit to the π^* orbital delocalized over the whole C^N moiety. It is interesting to note that the first and second singlet−singlet transitions for the closed forms of **1b**−**5b** are close in energy. The more intense transition (669−800 nm) can be assigned as IL [π(dithienylthiophene) → π^*(C^N)] transition ($S_0 \rightarrow S_1$ for **2b** and **5b**, and $S_0 \rightarrow S_2$ for **1b**, **3b** and **4b**), while the less intense transition can be assigned as LLCT [π(dithienylthiophene) → π^*(O^O)] transition.

Based on the TDDFT/CPCM calculations, the low-energy absorption band for the open forms in each complex centered at ~416−485 nm corresponds to the IL π−π^* transition of the C^N ligand with some mixing of MLCT [Pt(dπ) → π^*(C^N)] character. The weak absorption tail that is only observed in some of the hfac complexes at ~473−520 nm is ascribed to the LLCT [π(C^N) → π^*(O^O)] transition. As shown in Table S4 (SI), the IL π−π^* transition is red-shifted upon going from the nonsubstituted complexes (**1** and **4**) to the CF_3-substituted complexes (**2** and **5**). The energy level of both the π orbital (HOMO for **1a**−**5a** and **1b**−**5b**) and π^* orbital (LUMO for **1a**−**5a** and LUMO+1 for **1b**−**5b**) of the C^N ligands is decreased with the electron-withdrawing CF_3 group attached to the pyridyl unit of the C^N ligand. However, as the π^* orbital is more localized on the pyridyl unit (see Table S2 in SI), the decrease in the π^* orbital energy level will be to a larger extent, leading to a smaller π−π^* energy gap. The transition energy to the IL π−π^* excited state in the CH_3-substituted complexes **3a** and **3b** is found to be roughly the same as the nonsubstituted complexes **1a** and **1b**, which is in agreement with the observed trend in the low-energy absorption band of **1** and **3** and in other related (C^N)Pt(O^O) system.[9e] One can also see that the IL π−π^* transition is red-shifted upon going from the thienylpyridyl complexes **1** and **2** to the thieno[3,2-*b*]thienylpyridyl complexes **4** and **5**, respectively. The result is attributed to the increase in extended π-conjugation upon introduction of a fused thiophene unit on the thienyl moeity, leading to the higher-energy π orbital and lower-energy π^* orbital. In general, the calculated wavelengths for the IL π−π^* transition in the order of **1a** (406 nm) ≈ **3a** (409 nm) < **2a** (424 nm) and **4a** (427 nm) < **5a** (446 nm) for the acac complexes and **1b** (406 nm) ≈ **3b** (407 nm) < **2b** (429 nm) and **4b** (428 nm) < **5b** (449 nm) for the hfac complexes are in agreement with the observed trend of the experimental λ_{max} in the low-energy absorption band.

As depicted in Table S5 (SI), the low-energy absorption band for the closed form is due to the IL $\pi-\pi^*$ transition from the π orbital localized on the condensed ring of the dithienylthiophene unit to the π^* orbital delocalized over the entire C^N moiety. In general, the IL $\pi-\pi^*$ transition is calculated to be red-shifted upon going from the acac complexes to the corresponding hfac complexes, which is due to a larger decrease in the π^* orbital energy level relative to the π orbital energy level upon introduction of the more electron-deficient hfac ligand. Furthermore, the energy of the IL $\pi-\pi^*$ transition for the closed form is calculated to be in the order **3a** > **1a** > **2a** and **3b** > **1b** > **2b**, which is attributed to a larger decrease and increase in the π^* orbital energy level relative to the π orbital energy level with the electron-withdrawing CF_3 and electron-donating CH_3 group attached to the pyridyl unit, respectively. Since the π orbital has a very small contribution from the pyridyl unit, the energy level will be less affected by the substituents attached to it (see Table S2 in SI). Interestingly, the IL $\pi-\pi^*$ transition is found to be blue-shifted upon going from the thienylpyridyl complexes **1** and **2** to the thieno[3,2-*b*]thienylpyridyl complexes **4** and **5**, which is in contrast to the trend found in the corresponding open forms. The findings may be rationalized as follows. For the acac analogues, on changing from the open form to the closed form, the HOMO energy level is increased and the LUMO energy level is decreased due to the increase in the extent of π-conjugation. As shown in Table S3 (SI) , the magnitude of the change in the HOMO energy level is larger than that of the LUMO energy level from the open forms to the closed forms. These probably arise from the fact that the HOMO of the closed form is localized on the condensed ring of the dithienylthiophene unit while the LUMO is delocalized onto the entire C^N ligand, and thus a larger change would be expected in the HOMO level upon ring closing. One could also see that the HOMO energy level is increased to a greater extent for the thienylpyridyl complexes (by 1.13−1.16 eV) when compared with the corresponding thieno-[3,2-*b*]thienylpyridyl complexes (by 0.81−0.97 eV), while the extent of the decrease in the LUMO energy level for the two classes of complexes is more or less the same, leading to a smaller HOMO−LUMO energy separation in the former. Since the HOMO of the open forms in the thienylpyridyl complexes has a larger contribution from the π orbital of the dithienylthiophene unit, a larger increase could be found in the HOMO level (see Table S2 in SI). A similar explanation could be applied for the hfac complexes (HOMO−LUMO energy separation for **2b** and **5b** and HOMO−LUMO+1 energy separation for **1b** and **4b**).

As mentioned previously, the emission of the open form in **1**−**5** is originated from excited states of triplet parentage. Table S6 (SI) lists the first singlet−triplet transitions of the open forms. The lowest-energy transitions for the acac series **1a**−**5a** and hfac series **1b**−**5b** are contributed from HOMO → LUMO and HOMO → LUMO+1 excitation, respectively, in which both involve IL $\pi-\pi^*$ transition of the C^N ligand mixed with MLCT [Pt(dπ) → π^*(C^N)] transition. The transition wavelengths of the ^{3}IL/^{3}MLCT triplet excited state for the acac and hfac complexes are computed in the range of 580−638 nm and 581−643 nm, respectively. On the basis of the major excitations in the T_1 excited state obtained from the TDDFT calculation, the unrestricted Kohn−Sham approach (UPBE0) was used to optimize the lowest-energy triplet excited state in order to determine the nature of the triplet excited state at the relaxed molecular geometry. The major geometrical changes of the triplet excited state relative to the ground-state structure occur mainly in thpy and tthpy core of the C^N ligand. The lower-energy and higher-energy singly occupied molecular orbitals (SOMOs) of the triplet excited state are mainly the π orbital of the C^N ligand mixed with the metal orbital and the π^* orbital of the C^N ligand, respectively, which indicates that the triplet excited state consists of IL $\pi-\pi^*$ character of the C^N ligand with a slight mixing of MLCT character, further supporting the assignment from the photophysical study. The spatial plot of the spin density of the triplet excited state in each complex reveals that the spin density is localized mainly on the thpy/tthpy core with some on the metal center (see complexes **1a** and **4a** in the Figure S13, SI).

CONCLUSION

A new series of photochromic cyclometalated platinum(II) complexes has been successfully synthesized and structurally characterized. Their photophysical, photochromic and electrochemical properties have been studied. Most of them exhibit strong red ^{3}IL/^{3}MLCT phosphorescence in the solid state, in solution and in glass at 77 and 298 K. Moreover, the photochromic and photophysical properties can be easily modulated by changing the substituents on the pyridyl ring, the nature of the ancillary β-diketonate ligand at the platinum center and the extension of the π-conjugation on the C^N ligand without the need for tedious modification of the dithienylethene framework. This present work provides deeper insights for the future design of metal-containing photochromic materials.

EXPERIMENTAL SECTION

Materials and Reagents. Tetrakis(triphenylphosphine)palladium(0)[18] as catalyst for Suzuki cross-coupling, 2,3-bis(2,5-dimethylthiophen-3-yl)-thieno[3,2-*b*]thiophene[6j] and 2,3-bis(2,5-dimethylthiophen-3-yl)thiophene[6j] were prepared according to literature procedures. Tetrahydrofuran (THF, Lab Scan, AR) was distilled over sodium before use. All other solvents and reagents were of analytical grade and were used as received.

Physical Measurements and Instrumentation. ^{1}H NMR spectra were recorded using either a Bruker DPX-300 (300 MHz) or a Bruker AV400 (400 MHz) NMR spectrometer at 298 K. Chemical shifts (δ, ppm) for ^{1}H NMR and ^{19}F NMR were recorded relative to tetramethylsilane (Me_4Si) and trichlorofluoromethane ($CFCl_3$), respectively. Positive-ion fast atom bombardment (FAB) mass spectra were recorded on a Finnigan MAT 95 mass spectrometer. Elemental analyses of the new compounds were performed on a Carlo Erba 1106 elemental analyzer at the Institute of Chemistry, Chinese Academy of Sciences, Beijing.

UV−Vis absorption spectra were recorded using a Hewlett-Packard 8452A diode array spectrophotometer. Photoirradiation was carried out using a 300 W Oriel Corporation model 60011 Xe (ozone-free) lamp, and monochromic light was obtained by passing the light through an Applied Photophysics F3.4 monchromator. All measurements were conducted at room temperature.

Steady-state emission and excitation spectra at room temperature and 77 K were recorded on a Spex Fluorolog-2 model F111 spectrofluorometer. For solution emission and excitation spectra, samples were degassed on a high-vacuum line in a degassing cell with 10 cm^3 Pyrex round-bottomed flask connected by a side arm to a 1-cm quartz fluorescence cuvette and sealed from the atmosphere by a Rotaflo HP6/6 quick release Teflon stopper. Solutions were rigorously degassed with no fewer than four freeze−pump−thaw cycles prior to the measurements. Solid-state emission and excitation spectra at room temperature were recorded with solid samples loaded in a quartz tube inside a quartz-walled Dewar

flask. Solid samples at low temperature (77 K) and in butyronitrile glass at 77 K were recorded similarly, with liquid nitrogen inside the optical Dewar flask. Excited state lifetimes of solution, solid, and glass samples were measured using a conventional laser system. The excitation source used was a 355-nm output (third harmonic, 8 ns) of a Spectra-Physics Quanta-Ray Q-switched GCR-150-10 pulsed Nd:YAG laser (10 Hz). Luminescence decay traces at a selected wavelength were detected by a Hamamatsu R928 photomultiplier tube connected to a 50 Ω load resistor and the voltage signal recorded on a Tekronix model TDS620A digital oscilloscope (500 MHz, 2 GS/s). The lifetime (τ) determination was achieved by the single exponential fitting of the luminescence decay traces with the equation, $I(t) = I_0 \exp(-t/\tau)$, where $I(t)$ and I_0 refer to the luminescence intensity at the time = t and time = 0, respectively. Luminescence quantum yield was measured by the optical dilute method developed by Demas and Crosby.[19a] A degassed aqueous solution of $[Ru(bpy)_3]Cl_2$ was used as standard[19b,c] at 298 K.

Chemical actinometry was employed for the photochemical quantum yield determination.[20] Incident light intensities were taken from the average values measured just before and after each photolysis experiment using ferrioxalate actinometry and Reinecke's salt actinometry.[20] In the determination of the photochemical quantum yield, the sample solutions were prepared at concentrations with absorbance slightly greater than 2.0 at the excitation wavelength. The quantum yield was determined at a small percentage of conversion by monitoring the initial rate of change of absorbance ($\Delta A/\Delta t$) in the absorption maximum of the closed forms in the visible region.

Cyclic voltammetric measurements were performed by using a CH Instrument, Inc., model CHI620 electrochemical analyzer interfaced to a personal computer. The electrolytic cell used was a conventional two-compartment cell. The salt bridge of the reference electrode was separated from the working electrode compartment by a vycor glass. Electrochemical measurements were performed in dichloromethane solution with 0.1 mol dm^{-3} $^nBu_4NPF_6$ as supporting electrolyte at room temperature. The reference electrode was a $Ag/AgNO_3$ (0.1 M in acetonitrile) electrode, and the working electrode was a glassy carbon (CH Instrument) electrode with a platinum wire as a counter electrode in a compartment separated from the working electrode by a sintered-glass frit. The ferrocenium/ferrocene couple ($FeCp_2^{+/0}$) was used as the internal reference.[21] All solutions for electrochemical studies were deaerated with prepurified argon gas before measurement.

Crystal Structure Determination. Single crystals of complexes **1a**−**3a**, **1b**, and **4b** suitable for X-ray diffraction studies were grown by layering of methanol onto a concentrated dichloromethane solution of the complexes. The X-ray diffraction data were collected on a Bruker Smart CCD 1000 using graphite monochromatized Mo−K_α radiation (λ = 0.71073 Å). Raw frame data were integrated with SAINT[22] program. Semiempirical absorption corrections with SADABS[23] were applied. The structure was solved by direct methods employing SHELXS-97 program[24] on PC. Pt, S and many non-hydrogen atoms were located according to the direct methods. The positions of the other non-hydrogen atoms were found after successful refinement by full-matrix least-squares using program SHELXL-97[24] on PC. The positions of H atoms were calculated based on riding mode with thermal parameters equal to 1.2 times that of the associated C atoms, and participated in the calculation of final R-indices.

Synthesis. *4,4,5,5-Tetramethyl-2-(2,2″,5,5″-tetramethyl-[3,2′:3′,3″-terthiophen]-5′-yl)-1,3,2-dioxaborolane (Bpin-thiophene-DTE).* This was prepared according to a literature procedure[12] with slight modifications and the reaction was performed under anhydrous condition using standard Schlenk technique. To a well stirred solution of bis(pinacolato)diboron (2 g, 7.9 mmol) and 2,3-bis(2,5-dimethylthiophen-3-yl)thiophene (2 g, 6.6 mmol) in anhydrous degassed hexane (50 mL) was added (1,5-cyclooctadiene)(methoxy)iridium(I) dimer (80 mg, 0.12 mmol) and 4, 4′-di-*tert*-butyl-2,2′-bipyridine (80 mg, 0.30 mmol). The resulting mixture was heated under reflux overnight in the dark. This was then extracted with dichloromethane. The combined extracts were washed with brine and water, and finally dried over anhydrous magnesium sulfate. After filtration and removal of the solvent, the crude product was purified by column chromatography on silica gel (70−230 mesh) using hexane−dichloromethane (4:1 v/v) as the eluent. Further purification was achieved by recrystallization from a minimal amount of hexane and stored at −18 °C to afford the product as white crystals. Yield: 2.0 g, 4.6 mmol; 71%. ^{1}H NMR (400 MHz, $CDCl_3$, 298 K): δ 1.28 (s, 12H, $-CH_3$), 1.92 (s, 3H, $-CH_3$), 1.98 (s, 3H, $-CH_3$), 2.28 (s, 6H, $-CH_3$), 6.35 (s, 1H, dimethylthienyl), 6.38 (s, 1H, dimethylthienyl), 7.48 (s, 1H, thienyl). Positive-ion EI mass spectrum: m/z 430 $\{M\}^+$.

2-(5,6-Bis(2,5-dimethylthiophen-3-yl)thieno[3,2-b]thiophen-2-yl)-4,4,5,5-tetramethyl-1,3,2-dioxaborolane (Bpin-thienothiophene-DTE). This was synthesized according to a procedure similar to that of Bpin-thiophene-DTE except 2,3-bis(2,5-dimethylthiophen-3-yl)thieno[3,2-*b*]-thiophene (2.37 g, 6.6 mmol) was used in place of 2,3-bis(2,5-dimethylthiophen-3-yl)thiophene. Pale-green crystals were obtained. Yield 2.2 g, 4.5 mmol; 69%. ^{1}H NMR (400 MHz, $CDCl_3$, 298 K): δ 1.36 (s, 12H, $-CH_3$), 1.96 (s, 3H, $-CH_3$), 2.05 (s, 3H, $-CH_3$), 2.38 (s, 3H, $-CH_3$), 2.41(s, 3H, $-CH_3$), 6.66 (s, 1H, dimethylthienyl), 6.71 (s, 1H, dimethylthienyl), 7.74 (s, 1H, thienothienyl). Positive-ion EI mass spectrum: m/z 486 $\{M\}^+$.

2-(2,2″,5,5″-Tetramethyl-[3,2′:3′,3″-terthiophen]-5′-yl)pyridine (thpy-DTE). The target compound was synthesized according to standard Suzuki coupling reaction[13] under a heterogeneous mixture of water and THF. To a solution mixture of Bpin-thiophene-DTE (1 g, 2.3 mmol), 2-bromopyridine (0.367 g, 2.3 mmol) and tetrakis(triphenylphosphine)palladium(0) (0.135 g, 0.12 mmol) in THF (80 mL) was added aqueous cesium carbonate solution (2 M, 3.03 g, 4.65 mL 9.3 mmol). The reaction mixture was vigorously stirred and refluxed in the dark overnight. This was then extracted with dichloromethane. The combined extracts were washed with brine and water, and finally dried over anhydrous magnesium sulfate. After filtration and removal of the solvent, the crude product was purified by column chromatography on silica gel (70−230 mesh) using hexane−dichloromethane (1:1 v/v) as the eluent. Further purification was achieved by recrystallization from a minimal amount of hexane and stored at −18 °C to afford the product as white crystals. Yield: 750 mg, 1.97 mmol; 85%. ^{1}H NMR (400 MHz, $CDCl_3$, 298 K): δ 2.04 (s, 3H, $-CH_3$), 2.11 (s, 3H, $-CH_3$), 2.37 (s, 3H, $-CH_3$), 2.39(s, 3H, $-CH_3$), 6.49 (s, 2H, dimethylthienyl), 7.07−7.18 (m, 1H, 5-pyridyl), 7.51 (s, 1H, thienyl), 7.55−7.73 (m, 2H, 3-pyridyl, 4-pyridyl), 8.57 (ddd, J = 4.9, 1.6, 1.0 Hz, 1H, 6-pyridyl). Positive-ion EI mass spectrum: m/z 381 $\{M\}^+$.

2-(2,2″,5,5″-Tetramethyl-[3,2′:3′,3″-terthiophen]-5′-yl)-5-(trifluoromethyl)-pyridine (CF_3-thpy-DTE). This was synthesized according to a procedure similar to that of thpy-DTE except 2-bromo-5-(trifluoromethyl)-pyridine (0.520 g, 2.3 mmol) was used in place of 2-bromopyridine. Pale green crystals were obtained. Yield: 904 mg, 2.09 mmol; 91%. ^{1}H NMR (400 MHz, $CDCl_3$, 298 K): δ 2.04 (s, 3H, $-CH_3$), 2.11 (s, 3H, $-CH_3$), 2.37 (s, 3H, $-CH_3$), 2.40(s, 3H, $-CH_3$), 6.49 (s, 1H, dimethylthienyl), 6.50 (s, 1H, dimethylthienyl), 7.60 (s, 1H, thienyl), 7.72 (d, J = 8.4 Hz, 1H, 4-pyridyl), 7.89 (dd, J = 8.4, 1.9 Hz, 1H, 3-pyridyl), 8.81 (s, 1H, 6-pyridyl). Positive-ion EI mass spectrum: m/z 449 $\{M\}^+$.

5-Methyl-2-(2,2″,5,5″-tetramethyl-[3,2′:3′,3″-terthiophen]-5′-yl)pyridine (Me-thpy-DTE). This was synthesized according to a procedure similar to that of thpy-DTE except 2-bromo-5-methylpyridine (0.396 g, 2.3 mmol) was used in place of 2-bromopyridine. White crystals were obtained. Yield: 800 mg, 2.02 mmol; 88%. ^{1}H NMR (300 MHz, $CDCl_3$, 298 K): δ 2.03 (s, 3H, $-CH_3$), 2.10 (s, 3H, $-CH_3$), 2.34 (s, 3H, pyridyl-CH_3), 2.37 (s, 3H, $-CH_3$), 2.39(s, 3H, $-CH_3$), 6.49 (s, 2H, dimethylthienyl), 7.44 (s, 1H, thienyl), 7.48 (d, J = 8.1 Hz, 1H, 3-pyridyl), 7.55 (d, J = 8.1 Hz, 1H, 4-pyridyl), 8.40 (s, 1H, 6-pyridyl). Positive-ion EI mass spectrum: m/z 395 $\{M\}^+$.

2-(5,6-Bis(2,5-dimethylthiophen-3-yl)thieno[3,2-b]thiophen-2-yl)-pyridine (tthpy-DTE). This was synthesized according to a procedure similar to that of thpy-DTE except Bpin-thienothiophene-DTE (1.12 g, 2.3 mmol) was used in place of Bpin-thiophene-DTE. White crystals were obtained. Yield: 776 mg, 1.77 mmol; 77%. ^{1}H NMR (300 MHz, $CDCl_3$, 298 K): δ 1.99 (s, 3H, $-CH_3$), 2.09 (s, 3H, $-CH_3$), 2.41 (s, 3H, $-CH_3$), 2.44 (s, 3H, $-CH_3$), 6.57 (s, 1H, dimethylthienyl), 6.77 (s, 1H, dimethylthienyl), 7.17 (dd, J = 8.6, 4.8 Hz, 1H, 5-pyridyl), 7.64−7.74 (m, 2H, 3-pyridyl, 4-pyridyl), 7.77 (s, 1H, thienothienyl), 8.58 (d, J = 4.9 Hz, 1H, 6-pyridyl). Positive-ion EI mass spectrum: m/z 437 $\{M\}^+$.

2-(5,6-Bis(2,5-dimethylthiophen-3-yl)thieno[3,2-b]thiophen-2-yl)-5-(trifluoromethyl)pyridine (CF_3-tthpy-DTE). This was synthesized according to a procedure similar to that of CF_3-thpy-DTE except Bpin-thienothiophene-DTE (1.12 g, 2.3 mmol) was used in place of Bpin-thiophene-DTE. Pale yellow crystals were obtained. Yield: 878 mg, 1.74 mmol; 76%. ^{1}H NMR (400 MHz, $CDCl_3$, 298 K): δ 1.98 (s, 3H, $-CH_3$), 2.08 (s, 3H, $-CH_3$), 2.39 (s, 3H, $-CH_3$), 2.43 (s, 3H, $-CH_3$), 6.56 (s, 1H, dimethylthienyl), 6.74 (s, 1H, dimethylthienyl), 7.75 (d, J = 8.4 Hz, 1H, 4-pyridyl), 7.84 (s, 1H, thienothienyl), 7.89 (dd, J = 8.4, 2.1 Hz, 1H, 3-pyridyl), 8.79 (s, 1H, 6-pyridyl). Positive-ion EI mass spectrum: m/z 505 $\{M\}^+$.

[Pt(thpy-DTE)(Hthpy-DTE)Cl]. The complex was prepared according to a literature procedure[9e] with slight modifications and the reaction was performed under nitrogen. To a solution of thpy-DTE (300 mg, 0.79 mmol) in 2-ethoxyethanol (30 mL) and water (10 mL) mixture was added potassium tetrachloroplatinate(II) (104 mg, 0.32 mmol). The resulting mixture was stirred at 80 °C for 24 h. This was then extracted with dichloromethane. The combined extracts were washed with brine and water, and finally dried over anhydrous magnesium sulfate. After filtration and removal of the solvent, the crude product was purified by column chromatography on silica gel (70−230 mesh) using dichloromethane as the eluent. Further purification was achieved by recrystallization from layering of methanol onto a concentrated dichloromethane solution of the complex to afford orange crystals. Yield: 240 mg, 0.24 mmol; 76%. Isomer 1: ^{1}H NMR (400 MHz, $CDCl_3$, 298 K): δ 1.58 (s, 3H, $-CH_3$), 1.87 (s, 3H, $-CH_3$), 2.04 (s, 6H, $-CH_3$), 2.14 (s, 3H, $-CH_3$), 2.23 (s, 3H, $-CH_3$), 2.32 (s, 3H, $-CH_3$), 2.35 (s, 3 H, $-CH_3$), 6.05 (s, 1H, dimethylthienyl), 6.07 (s, 1H, dimethylthienyl), 6.38 (s, 1H, dimethylthienyl), 6.42 (s, 1H, dimethylthienyl), 6.74 (t, J = 6.1 Hz, 1H, pyridyl), 6.87−7.00 (m, 1H, pyridyl), 7.28−7.36 (m, 1H, pyridyl), 7.44−7.63 (m, 2H, pyridyl), 7.65−7.74 (m, 1H, pyridyl), 8.11(s, 1H, thienyl), 8.44 (d, J = 5.4 Hz, 1H, 6-pyridyl), 9.55 (d, J = 5.7 Hz, 1H, 6-pyridyl). Isomer 2: ^{1}H NMR (400 MHz, $CDCl_3$, 298 K): δ 1.89 (s, 3H, $-CH_3$), 1.97 (s, 3H, $-CH_3$), 2.01 (s, 6H, $-CH_3$), 2.15 (s, 3H, $-CH_3$), 2.20 (s, 3H, $-CH_3$), 2.28 (s, 3H, $-CH_3$), 2.36 (s, 3 H, $-CH_3$), 5.94 (s, 1H, dimethylthienyl), 5.97 (s, 1H, dimethylthienyl), 6.25 (s, 1H, dimethylthienyl), 6.34 (s, 1H, dimethylthienyl), 6.68−7.00 (m, 1H, pyridyl), 7.06 (t, J = 6.1 Hz, 1H, pyridyl), 7.28−7.36 (m, 1H, pyridyl), 7.44−7.63 (m, 2H, pyridyl), 7.65−7.74 (m, 1H, pyridyl), 7.75 (s, 1H, thienyl), 9.19 (d, J = 5.3 Hz, 1H, 6-pyridyl), 9.65 (d, J = 5.8 Hz, 1H, 6-pyridyl). Positive FAB mass spectrum: m/z 992 $\{M\}^+$, 957 $\{M - Cl\}^+$, 574 $\{M - Cl - Hthpy\text{-}DTE\}^+$.

[Pt(CF_3-thpy-DTE)(CF_3-Hthpy-DTE)Cl]. This was synthesized according to a procedure similar to that of [Pt(thpy-DTE)(Hthpy-DTE)Cl] except CF_3-thpy-DTE (341 mg, 0.79 mmol) was used in place of thpy-DTE. Reddish orange crystals were obtained. Yield: 240 mg, 0.210 mmol; 66%. Isomer 1: ^{1}H NMR (400 MHz, $CDCl_3$, 298 K): δ 1.92 (s, 3H, $-CH_3$), 1.98 (s, 3H, $-CH_3$), 2.03 (s, 3H, $-CH_3$), 2.19 (s, 3H, $-CH_3$), 2.20 (s, 3H, $-CH_3$), 2.30 (s, 3H, $-CH_3$), 2.37 (s, 6 H, $-CH_3$), 5.90 (s, 1H, dimethylthienyl), 5.95 (s, 1H, dimethylthienyl), 6.30 (s, 1H, dimethylthienyl), 6.35 (s, 1H, dimethylthienyl), 7.41 (d, J = 8.3 Hz, 1H, pyridyl), 7.59 (d, J = 8.7 Hz, 1H, pyridyl), 7.67−7.77 (m, 1H, pyridyl), 7.88−7.95 (m, 1H, pyridyl), 7.77 (s, 1H, thienyl), 9.45 (s, 1H, 6-pyridyl), 9.96 (s, 1H, 6-pyridyl). Isomer 2: ^{1}H NMR (400 MHz, $CDCl_3$, 298 K): δ 1.51 (s, 3H, $-CH_3$), 1.80 (s, 3H, $-CH_3$), 2.00 (s, 3H, $-CH_3$), 2.06 (s, 3H, $-CH_3$), 2.08 (s, 3H, $-CH_3$), 2.15 (s, 3H, $-CH_3$), 2.23 (s, 3H, $-CH_3$), 2.33 (s, 3H, $-CH_3$), 6.04 (s, 1H, dimethylthienyl), 6.14 (s, 1H, dimethylthienyl), 6.40 (s, 1H, dimethylthienyl), 6.43 (s, 1H, dimethylthienyl), 7.38 (d, J = 8.1 Hz, pyridyl), 7.67−7.77 (m, 2H, pyridyl), 7.88−7.95 (m, 1H, pyridyl), 8.14 (s, 1H, thienyl), 9.11 (s, 1H, 6-pyridyl), 9.86 (s, 1H, 6-pyridyl). Positive FAB mass spectrum: m/z 1129 $\{M\}^+$, 1092 $\{M - Cl\}^+$, 642 $\{M - Cl - CF_3 - Hthpy\text{-}DTE\}^+$.

[Pt(Me-thpy-DTE)(Me-Hthpy-DTE)Cl]. This was synthesized according to a procedure similar to that of [Pt(thpy-DTE)(Hthpy-DTE)Cl] except Me-thpy-DTE (313 mg, 0.79 mmol) was used in place of thpy-DTE. Orange crystals were obtained. Yield: 260 mg, 0.25 mmol; 80%. Isomer 1: ^{1}H NMR (400 MHz, $CDCl_3$, 298 K): δ 1.23 (s, 3H, $-CH_3$), 1.90 (s, 3H, $-CH_3$), 1.96 (s, 3H, $-CH_3$), 2.16 (s, 3H, $-CH_3$), 2.19 (s, 3H, $-CH_3$), 2.28 (s, 3H, $-CH_3$), 2.33 (s, 3H, $-CH_3$), 2.35 (s, 6H, $-CH_3$), 2.37 (s, 3H, $-CH_3$), 5.93 (s, 1H, dimethylthienyl), 5.96 (s, 1H, dimethylthienyl), 6.26 (s, 1H, dimethylthienyl), 6.34 (s, 1H, dimethylthienyl), 7.19−7.30 (m, 1H, pyridyl), 7.34−7.40 (m, 1H, pyridyl), 7.47−7.57 (m, 1H, pyridyl), 7.73 (s, 1H, thienyl), 9.08 (d, J = 5.8 Hz, 1H, 6-pyridyl), 9.47 (d, J = 5.8 Hz, 1H, 6-pyridyl). Isomer 2: ^{1}H NMR (400 MHz, $CDCl_3$, 298 K): δ 1.86 (s, 3H, $-CH_3$), 1.99 (s, 3H, $-CH_3$), 2.03 (s, 6H, $-CH_3$), 2.04 (s, 3H, $-CH_3$), 2.05 (s, 3H, $-CH_3$), 2.13 (s, 3H, $-CH_3$), 2.14 (s, 3H, $-CH_3$), 2.23 (s, 3H, $-CH_3$), 2.35 (s, 3H, $-CH_3$), 6.05 (s, 1H, dimethylthienyl), 6.11 (s, 1H, dimethylthienyl), 6.38 (s, 1H, dimethylthienyl), 6.44 (s, 1H, dimethylthienyl), 7.19−7.30 (m, 2H, pyridyl), 7.47−7.57 (m, 2H, pyridyl), 8.09 (s, 1H, thienyl), 8.68 (d, J = 5.8 Hz, 1H, 6-pyridyl), 9.37 (d, J = 5.8 Hz, 1H, 6-pyridyl). Positive FAB mass spectrum: m/z 1020 $\{M\}^+$, 985 $\{M - Cl\}^+$, 588 $\{M - Cl - Me - Hthpy\text{-}DTE\}^+$.

[Pt(tthpy-DTE)(Htthpy-DTE)Cl]. This was synthesized according to a procedure similar to that of [Pt(thpy-DTE)(Hthpy-DTE)Cl] except tthpy-DTE (346 mg, 0.79 mmol) was used instead of thpy-DTE. Reddish orange crystals were obtained. Yield: 260 mg, 0.210 mmol; 73%. ^{1}H NMR (300 MHz, $CDCl_3$, 298 K): δ 1.88 (s, 3H, $-CH_3$), 1.92 (s, 3H, $-CH_3$), 1.99 (s, 3H, $-CH_3$), 2.00 (s, 3H, $-CH_3$), 2.30 (s, 3H, $-CH_3$), 2.34 (s, 3H, $-CH_3$), 2.37 (s, 3H, $-CH_3$), 2.43 (s, 3H, $-CH_3$), 6.31 (s, 1H, dimethylthienyl), 6.48 (s, 1H, dimethylthienyl), 6.51 (s, 1H, dimethylthienyl), 6.61 (s, 1H, dimethylthienyl), 6.84−7.06 (m, 1H, pyridyl), 7.21 (d, J = 7.8 Hz, 1H, pyridyl), 7.30 (dd, J = 6.5, 1.8 Hz, 1H, pyridyl), 7.68 (td, J = 7.8, 1.5 Hz, 1H, pyridyl), 7.80−7.99 (m, 2H, pyridyl), 8.59 (s, 1H, thienothienyl), 9.31 (d, J = 5.7 Hz, 1H, 6-pyridyl), 9.48 (d, J = 5.7 Hz, 1H, 6-pyridyl). Positive FAB mass spectrum: m/z 1104 $\{M\}^+$, 1069 $\{M - Cl\}^+$, 631 $\{M - Cl - Htthpy\text{-}DTE\}^+$.

[Pt(CF_3-tthpy-DTE)(CF_3-Htthpy-DTE)Cl]. This was synthesized according to a procedure similar to that of [Pt(CF_3-thpy-DTE)(CF_3-Hthpy-DTE)Cl] except CF_3-tthpy-DTE (399 mg, 0.79 mmol) was used in place of CF_3-thpy-DTE. Reddish orange crystals were obtained. Yield: 307 mg, 0.247 mmol; 77%. ^{1}H NMR (400 MHz, $CDCl_3$, 298 K): δ 1.85 (s, 3H, $-CH_3$), 1.89 (s, 3H, $-CH_3$), 1.99 (s, 3H, $-CH_3$), 2.00 (s, 3H, $-CH_3$), 2.28 (s, 3H, $-CH_3$), 2.32 (s, 3H, $-CH_3$), 2.36 (s, 3 H, $-CH_3$), 2.40 (s, 3 H, $-CH_3$), 6.26 (s, 1H, dimethylthienyl), 6.47 (s, 1H, dimethylthienyl), 6.51 (s, 1H, dimethylthienyl), 6.58 (s, 1H, dimethylthienyl), 7.28 (d, J = 8.5 Hz, 1H, pyridyl), 7.88 (dd, J = 8.5, 1.8 Hz, 1H, pyridyl), 8.02 (d, J = 8.6 Hz, 1H, pyridyl), 8.13 (dd, J = 8.6, 2.0 Hz, 1H, pyridyl), 8.70 (s, 1H, thienothienyl), 9.57 (s, 1H, 6-pyridyl), 9.79 (s, 1H, 6-pyridyl). Positive FAB mass spectrum: m/z 1241 $\{M\}^+$, 1204 $\{M - Cl\}^+$, 699 $\{M - Cl - CF_3 - tthpy\text{-}DTE\}^+$.

*[Pt(thpy-DTE)(acac)] (**1a**).* The complex was prepared according to a literature procedure[9e] with slight modifications and the reaction was performed under nitrogen. To a solution of [Pt(thpy-DTE)(Hthpy-DTE)Cl] (300 mg, 0.30 mmol) in dichloromethane (50 mL) was added sodium acetylacetonate (369 mg, 3.0 mmol). The reaction mixture was vigorously stirred and refluxed in the dark, and the progress was monitored by thin layer chromatography (TLC). This was then

extracted with dichloromethane. The combined extracts were washed with brine and water and finally dried over anhydrous magnesium sulfate. After filtration and removal of the solvent, the crude product was purified by column chromatography on silica gel (70−230 mesh) using hexane−dichloromethane (3:1 v/v) as the eluent. Further purification was achieved by layering of methanol onto a concentrated dichloromethane solution of the complexes to afford orange crystals. Yield: 120 mg, 0.178 mmol; 59%. ^{1}H NMR (400 MHz, $CDCl_3$, 298 K): δ 1.51 (s, 3H, $-CH_3$), 1.94 (s, 3H, $-CH_3$), 2.06 (s, 3H, $-CH_3$), 2.17 (s, 3H, $-CH_3$), 2.32 (s, 6H, $-CH_3$), 5.37 (s, 1H, acac-H), 6.32 (s, 1H, dimethylthienyl), 6.48 (s, 1H, dimethylthienyl), 6.80−6.92 (m, 1H, 5-pyridyl), 7.24 (d, J = 8.2 Hz, 1H, 3-pyridyl), 7.65 (td, J = 8.1, 1.2 Hz, 1H, 4-pyridyl), 8.57 (d, J = 5.8 Hz, 1H, 6-pyridyl). Positive FAB mass spectrum: m/z 675 $\{M\}^+$, 575 $\{M - acac\}^+$. Elemental analyses, Found (%): C 46.50, H 3.71, N 2.02; Calcd (%) for $C_{26}H_{25}NO_2PtS_3$: C 46.28, H 3.73, N 2.08.

[Pt(CF_3-thpy-DTE)(acac)] (***2a***). This was synthesized according to a procedure similar to that of **1a** except [Pt(CF_3-thpy-DTE)(CF_3-Hthpy-DTE)Cl] (339 mg, 0.3 mmol) was used in place of [Pt(thpy-DTE)-(Hthpy-DTE)Cl]. Orange crystals of **2a** were obtained. Yield: 140 mg, 0.19 mmol; 63%. ^{1}H NMR (400 MHz, $CDCl_3$, 298 K): δ 1.54 (s, 3H, $-CH_3$), 1.97 (s, 3H, $-CH_3$), 2.06 (s, 3H, $-CH_3$), 2.19 (s, 3H, $-CH_3$), 2.32 (s, 3H, $-CH_3$), 2.33 (s, 6H, $-CH_3$), 5.40 (s, 1H, acac-H), 6.31 (s, 1H, dimethylthienyl), 6.46 (s, 1H, dimethylthienyl), 7.29 (d, J = 8.5 Hz, 1H, 4-pyridyl), 7.65 (dd, J = 8.5, 1.5 Hz, 1H, 3-pyridyl), 9.13 (s, 1H, 6-pyridyl). ^{19}F NMR (376.4 MHz, $CDCl_3$, 298 K): δ−62.20. Positive FAB mass spectrum: m/z 743 $\{M\}^+$, 642 $\{M - acac\}^+$. Elemental analyses, Found (%): C 43.26, H 3.24, N 1.71; Calcd (%) for $C_{27}H_{24}F_3NO_2PtS_3 \cdot 0.5H_2O$: C 43.14, H 3.35, N 1.86.

[Pt(Me-thpy-DTE)(acac)] (***3a***). This was synthesized according to a procedure similar to that of **1a** except [Pt(Me-thpy-DTE)(Me-Hthpy-DTE)Cl] (306 mg, 0.3 mmol) was used in place of [Pt(thpy-DTE)-(Hthpy-DTE)Cl]. Orange crystals of **3a** were obtained. Yield: 120 mg, 0.17 mmol; 58%. ^{1}H NMR (400 MHz, $CDCl_3$, 298 K): δ 1.50 (s, 3H, $-CH_3$), 1.95 (s, 3H, $-CH_3$), 2.05 (s, 3H, $-CH_3$), 2.17 (s, 3H, $-CH_3$), 2.32 (s, 6H, $-CH_3$), 2.35 (s, 6H, pyridyl-CH_3), 5.36 (s, 1H, acac-H), 6.31 (s, 1H, dimethylthienyl), 6.48 (s, 1H, dimethylthienyl), 7.15 (d, J = 8.2 Hz, 1H, 4-pyridyl), 7.65 (dd, J = 8.2, 1.3 Hz, 1H, 3-pyridyl), 8.64 (s, 1H, 6-pyridyl). Positive FAB mass spectrum: m/z 689 $\{M\}^+$, 587 $\{M - acac\}^+$. Elemental analyses, Found (%): C 46.22, H 3.93, N 2.17; Calcd (%) for $C_{27}H_{27}NO_2PtS_3 \cdot 0.5H_2O$: C 46.47, H 4.04, N 2.01.

[Pt(tthpy-DTE)(acac)] (***4a***). This was synthesized according to a procedure similar to that of **1a** except [Pt(tthpy-DTE)(Htthpy-DTE)Cl] (331 mg, 0.3 mmol) was used in place of [Pt(thpy-DTE)(Hthpy-DTE)Cl]. Orange crystals of **4a** were obtained. Yield: 125 mg, 0.17 mmol; 57%. ^{1}H NMR (400 MHz, $CDCl_3$, 298 K): δ1.98 (s, 3H, $-CH_3$), 2.03 (s, 3H, $-CH_3$), 2.07 (s, 3H, $-CH_3$), 2.08 (s, 3H, $-CH_3$), 2.39 (s, 3H, $-CH_3$), 2.43 (s, 3H, $-CH_3$), 5.53 (s, 1H, acac-H), 6.57 (s, 1H, dimethylthienyl), 6.68 (s, 1H, dimethylthienyl), 6.88 (ddd, J = 7.3, 5.9, 1.4 Hz, 1H, 5-pyridyl), 7.19 (d, J = 7.7 Hz, 1H, 3-pyridyl), 7.65 (td, J = 8.0, 1.5 Hz, 1H, 4-pyridyl), 8.77 (d, J = 5.2 Hz, 1H, 6-pyridyl). Positive FAB mass spectrum: m/z 731 $\{M\}^+$. Elemental analyses, Found (%): C 45.94, H 3.65, N 1.96; Calcd (%) for $C_{28}H_{25}NO_2PtS_4$: C 46.02, H 3.45, N 1.92.

[Pt(CF_3-tthpy-DTE)(acac)] (***5a***). This was synthesized according to a procedure similar to that of **1a** except [Pt(CF_3-tthpy-DTE)(CF_3-Htthpy-DTE)Cl] (372 mg, 0.3 mmol) was used in place of [Pt(thpy-DTE)(Hthpy-DTE)Cl]. Orange crystals of **5a** were obtained. Yield: 125 mg, 0.16 mmol; 52%. ^{1}H NMR (400 MHz, $CDCl_3$, 298 K): δ 1.98 (s, 3H, $-CH_3$), 2.07 (s, 3H, $-CH_3$), 2.08 (s, 3H, $-CH_3$), 2.09 (s, 3H, $-CH_3$), 2.39 (s, 3H, $-CH_3$), 2.43 (s, 3H, $-CH_3$), 5.56 (s, 1H, acac-H), 6.57 (s, 1H, dimethylthienyl), 6.67 (s, 1H, dimethylthienyl), 7.23 (d, J = 8.7 Hz, 1H, 4-pyridyl), 7.82 (d, J = 8.7 Hz, 3-pyridyl), 9.03 (s, 1H, 6-pyridyl). ^{19}F NMR (376.4 MHz, $CDCl_3$, 298 K): δ −62.14. Positive FAB mass spectrum: m/z 799 $\{M\}^+$, 700 $\{M - acac\}^+$. Elemental analyses, Found (%): C 43.44, H 3.02, N 1.92; Calcd (%) for $C_{29}H_{24}F_3NO_2PtS_4$: C 43.60, H 3.03, N 1.75.

[Pt(thpy-DTE)(hfacac)] (***1b***). This was synthesized according to a procedure similar to that of **1a** except sodium hexafluoroacetylacetonate (690 mg, 3.0 mmol) was used in place of sodium acetylacetonate. Red crystals of **1b** were obtained. Yield: 100 mg, 0.13 mmol; 42%. ^{1}H NMR (400 MHz, $CDCl_3$, 298 K): δ 1.98 (s, 3H, $-CH_3$), 2.17 (s, 3H, $-CH_3$), 2.31 (s, 6H, $-CH_3$), 6.18 (s, 1H, acac-H), 6.20 (s, 1H, dimethylthienyl), 6.39 (s, 1H, dimethylthienyl), 6.93 (t, J = 6.3 Hz, 1H, 5-pyridyl), 7.30 (d, J = 8.0 Hz, 1H, 3-pyridyl), 7.72 (t, J = 7.7 Hz, 1H, 4-pyridyl), 8.55 (d, J = 5.8 Hz, 1H, 6-pyridyl). ^{19}F NMR (376.4 MHz, $CDCl_3$, 298 K): δ −74.54, −75.43. Positive FAB mass spectrum: m/z 782 $\{M\}^+$, 574 $\{M - hfacac\}^+$. Elemental analyses, Found (%): C 39.68, H 2.62, N 1.79; Calcd (%) for $C_{26}H_{19}F_6NO_2PtS_3$: C 39.90, H 2.47, N 1.79.

[Pt(CF_3-thpy-DTE)(hfacac)] (***2b***). This was synthesized according to a procedure similar to that of **2a** except sodium hexafluoroacetylacetonate (690 mg, 3.0 mmol) was used in place of sodium acetylacetonate. Yellow crystals of **2b** were obtained. Yield: 97 mg, 0.11 mmol; 38%. ^{1}H NMR (400 MHz, $CDCl_3$, 298 K): δ 1.98 (s, 3H, $-CH_3$), 2.19 (s, 3H, $-CH_3$), 2.32 (s, 6H, $-CH_3$), 6.19 (s, 1H, acac-H), 6.21 (s, 1H, dimethylthienyl), 6.38 (s, 1H, dimethylthienyl), 7.36 (d, J = 8.4 Hz, 1H, 4-pyridyl), 7.89 (d, J = 8.6 Hz, 1H, 3-pyridyl), 8.84 (s, 1H, 6-pyridyl). ^{19}F NMR (376.4 MHz, $CDCl_3$, 298 K): δ −62.61, −74.55, −75.50. Positive FAB mass spectrum: m/z 850 $\{M\}^+$, 641 $\{M - hfacac\}^+$. Elemental analyses, Found (%): C 37.97, H 2.25, N 1.73; Calcd (%) for $C_{27}H_{18}F_9NO_2PtS_3$: C 38.12, H 2.13, N 1.65.

[Pt(Me-thpy-DTE)(hfacac)] (***3b***). This was synthesized according to a procedure similar to that of **3a** except sodium hexafluoroacetylacetonate (690 mg, 3.0 mmol) was used in place of sodium acetylacetonate. Orange crystals of **3b** were obtained. Yield: 92 mg, 0.12 mmol; 38%. ^{1}H NMR (400 MHz, $CDCl_3$, 298 K): δ 1.98 (s, 3H, $-CH_3$), 2.17 (s, 3H, $-CH_3$), 2.31 (s, 6H, $-CH_3$), 2.36 (s, 3H, $-CH_3$), 6.17 (s, 1H, acac-H), 6.19 (s, 1H, dimethylthienyl), 6.39 (s, 1H, dimethylthienyl), 7.20 (d, J = 6.9 Hz, 1H, 4-pyridyl), 7.54 (d, J = 7.0 Hz, 1H, 3-pyridyl), 8.34 (s, 1H, 6-pyridyl). ^{19}F NMR (376.4 MHz, $CDCl_3$, 298 K): δ −74.55, −75.50. Positive FAB mass spectrum: m/z 796 $\{M\}^+$, 588 $\{M - hfacac\}^+$. Elemental analyses, Found (%): C 40.70, H 2.79, N 1.72; Calcd (%) for $C_{27}H_{21}F_6NO_2PtS_3$: C 40.70, H 2.66, N 1.76.

[Pt(tthpy-DTE)(hfacac)] (***4b***). This was synthesized according to a procedure similar to that of **4a** except sodium hexafluoroacetylacetonate (690 mg, 3.0 mmol) was used in place of sodium acetylacetonate. Orange crystals of **4b** were obtained. Yield: 101 mg, 0.12 mmol; 40%. ^{1}H NMR (400 MHz, $CDCl_3$, 298 K): δ 1.98 (s, 3H, $-CH_3$), 2.12 (s, 3H, $-CH_3$), 2.39 (s, 3H, $-CH_3$), 2.45 (s, 3H, $-CH_3$), 6.29 (s, 1H, acac-H), 6.51 (s, 1H, dimethylthienyl), 6.68 (s, 1H, dimethylthienyl), 6.85 (t, J = 6.6 Hz, 1H, 5-pyridyl), 7.14 (d, J = 8.1 Hz, 1H, 3-pyridyl), 7.61 (t, J = 7.7 Hz, 1H, 4-pyridyl), 8.42 (d, J = 5.8 Hz, 1H, 6-pyridyl). ^{19}F NMR (376.4 MHz, $CDCl_3$, 298 K): δ −73.75, −75.22. Positive FAB mass spectrum: m/z 839 $\{M\}^+$. Elemental analyses, Found (%): C 39.58, H 2.46, N 1.79; Calcd (%) for $C_{28}H_{19}F_6NO_2PtS_4 \cdot 0.5H_2O$: C 39.67, H 2.38, N 1.65.

[Pt(CF_3-tthpy-DTE)(hfacac)] (***5b***). This was synthesized according to a procedure similar to that of **5a** except sodium hexafluoroacetylacetonate (690 mg, 3.0 mmol) was used in place of sodium acetylacetonate. Orange crystals of **5b** were obtained. Yield: 107 mg, 0.12 mmol; 39%. ^{1}H NMR (400 MHz, $CDCl_3$, 298 K): δ 1.97 (s, 3H, $-CH_3$), 2.13 (s, 3H, $-CH_3$), 2.39 (s, 3H, $-CH_3$), 2.45 (s, 3H, $-CH_3$), 6.35 (s, 1H, acac-H), 6.50 (s, 1H, dimethylthienyl), 6.68 (s, 1H, dimethylthienyl), 7.21 (d, J = 8.1 Hz, 1H, 4-pyridyl), 7.79 (d, J = 8.5 Hz, 1H, 3-pyridyl), 8.70 (s, 1H, 6-pyridyl). ^{19}F NMR (376.4 MHz, $CDCl_3$, 298 K): δ −62.56, −73.68, −75.29. Positive FAB mass spectrum: m/z 906 $\{M\}^+$, 700 $\{M - hfacac\}^+$. Elemental analyses, Found (%): C 38.02, H 2.15, N 1.53; Calcd (%) for $C_{29}H_{18}F_9NO_2PtS_4 \cdot 0.5H_2O$: C 38.03, H 2.09, N 1.53.

Computational Details. Calculations were carried out using the *Gaussian03* software package.[25] Geometry optimizations were performed for the ground-state structures of the open and closed forms in complexes **1a**−**5a** and **1b**−**5b** with no symmetry restriction by using the density functional theory (DFT) at the hybrid Perdew, Burke, and Ernzerhof functional (PBE0)[26] level of theory with a pruned (99,590) grid. For the open forms, only photochemically active antiparallel conformation was considered. Although there are several possible conformers for the open and closed forms regarding the orientation of the peripheral thiophene rings, only the conformation of the two forms shown in Figure S11 (SI) for the thienylpyridyl and thieno[3,2-*b*]-thienylpyridyl complexes were considered in the study. On the basis of the ground-state optimized geometries in the gas phase, the nonequilibrium time-dependent TD-DFT method,[27] at the same level associated with conductor-like polarizable continuum model (CPCM)[28] using benzene as the solvent, was employed to compute the singlet−singlet and singlet−triplet transitions in the two forms of all the complexes. On the basis of the major excitation in the first lowest-lying singlet−triplet transition from the TDDFT calculation, the unrestricted UPBE0 was used to optimize the lowest triplet excited state of the open forms starting from the optimized ground-state structure. The Stuttgart effective core potentials (ECPs) and the associated basis set were applied to describe for Pt[29] with *f*-type polarization functions ($\xi = 0.993$),[30] while the 6-31G(d,p) basis set[31] was used for all other atoms. Vibrational frequency calculations were performed for all stationary points to verify that each was a minimum (NIMAG = 0) on the potential energy surface.

■ ASSOCIATED CONTENT

Supporting Information. Selected structural parameters of the optimized structures, percentage contribution of selected MOs, orbital energies, selected TDDFT/CPCM singlet−singlet and singlet−triplet transitions, synthetic pathway of complexes **1a**−**5a** and **1b**−**5b**, perspective views of **2a**, **3a** and **1b**, crystal packing diagrams of complexes **1b** and **4b**, cyclic voltammograms for **2a** and **2b**, electronic absorption spectra of the open forms of **1a** and **1b**, normalized electronic absorption spectra of the open form of **1a** in different solvents, absorption energy of the open form of **1a** in different solvents versus Dimroth's solvent parameter, normalized excitation spectra of the open forms of **1a**−**3a**, normalized corrected emission spectra of the open forms of **4a** and **4b**, Arrhenius plot for the thermal backward reaction of the closed form of **1a**, optimized geometries of **1a** and **4a**, spatial plots of the HOMO and LUMO in **4**, isocontour plot of the spin density in **1a** and **4a**, complete ref 25, and Cartesian coordinates of the optimized structures. This material is available free of charge via the Internet at http://pubs.acs.org.

■ AUTHOR INFORMATION

Corresponding Author
wwyam@hku.hk

■ ACKNOWLEDGMENT

V.W.-W.Y. acknowledges support from The University of Hong Kong under the Distinguished Research Achievement Award Scheme and the URC Strategic Research Theme on Molecular Materials. This work has been supported by the University Grants Committee Areas of Excellence Scheme (AoE/P-03/08). J.C.-C.C. acknowledges the receipt of a postgraduate studentship from The University of Hong Kong. We are grateful to Dr. L. Szeto for her assistance in X-ray crystal structure data collection and determination, and the Computer Center of The University of Hong Kong for providing computational resources, which were supported by a Hong Kong UGC Special Equipment Grant (SEG HKU09).

■ REFERENCES

(1) (a) Irie, M. *Chem. Rev.* **2000**, *100*, 1685. (b) Tian, H.; Yang, S. *Chem. Soc. Rev.* **2004**, *33*, 85. (c) Kellogg, R. M.; Greon, M. B.; Wynberg, H. *J. Org. Chem.* **1967**, *32*, 3093. (d) Raymo, F. M.; Tomasulo, M. *Chem. Soc. Rev.* **2005**, *34*, 327. (e) Tian, H.; Wang, S. *Chem. Commun.* **2007**, 781.

(2) (a) Otsuki, J.; Omokawa, N.; Yoshiba, K.; Akasaka, T.; Suenobu, T.; Takido, T.; Araki, K.; Fukuzumi, S. *Inorg. Chem.* **2003**, *42*, 3057. (b) Nishihara, H. *Bull. Chem. Soc. Jpn.* **2004**, *77*, 407. (c) Sakamoto, R.; Murata, M.; Jume, S.; Sampei, H.; Sugimoto, M.; Nishihara, H. *Chem. Commun.* **2005**, 1215. (d) Nishihara, H. *Coord. Chem. Rev.* **2005**, *249*, 1468. (e) Einaga, Y.; Mikami, R.; Akitsu, T.; Li, G. *Thin Solid Films* **2005**, 230. (f) Pratihar, P.; Mondal, T. K.; Patra, A. K.; Sinha, C. *Inorg. Chem.* **2009**, *48*, 2760.

(3) (a) Zarnegar, P. P.; Whitten, D. G. *J. Am. Chem. Soc.* **1971**, *93*, 3776. (b) Zarnegar, P. P.; Bock, C. R.; Whitten, D. G. *J. Am. Chem. Soc.* **1973**, *95*, 4361. (c) Yam, V. W.-W.; Lau, V. C. Y.; Wu, L. X. *J. Chem. Soc., Dalton Trans.* **1998**, 1461. (d) Sun, S. S.; Robson, E.; Dunwoody, N.; Silva, A. S.; Brinn, I. M.; Lees, A. J. *Chem. Commun.* **2000**, 201. (e) Lewis, J. D.; Perutz, R. N.; Moore, J. N. *Chem. Commun.* **2000**, 1865. (f) Yam, V. W.-W.; Yang, Y.; Zhang, J.; Chu, B. W.-K.; Zhu, N. *Organometallics* **2001**, *20*, 4911. (g) Yutaka, T.; Mori, I.; Kurihara, M.; Mizutani, J.; Tamai, N.; Kawai, T.; Irie, M.; Nishihara, H. *Inorg. Chem.* **2002**, *41*, 7143. (h) Wenger, O. S.; Henling, L. M.; Day, M. W.; Winkler, J. R.; Gray, H. B. *Inorg. Chem.* **2004**, *43*, 2043. (i) Nishihara, H. *Bull. Chem. Soc. Jpn.* **2004**, *77*, 407. (j) Busby, M.; Matousek, P.; Towrie, M.; Vlček, A., Jr. *J. Phys. Chem. A* **2005**, *109*, 3000.

(4) (a) Takayama, K.; Matsuda, K.; Irie, M. *Chem.—Eur. J.* **2003**, *9*, 5605. (b) Matsuda, K.; Takayama, K.; Irie, M. *Inorg. Chem.* **2004**, *43*, 482. (c) Morimoto, M.; Miyasaka, H.; Yamashita, M.; Irie, M. *J. Am. Chem. Soc.* **2009**, *131*, 9823. (d) Matsuda, K.; Takayama, K.; Irie, M. *Chem. Commun.* **2001**, 363. (e) Irie, M. *Chem. Rev.* **2000**, *100*, 1685.

(5) (a) Murguly, E.; Norsten, T. B.; Branda, N. R. *Angew. Chem., Int. Ed.* **2001**, *40*, 1752. (b) Fraysse, S.; Coudret, C.; Launay, J. P. *Eur. J. Inorg. Chem.* **2000**, 1581. (c) Fernández-Acebes, A.; Lehn, J. M. *Adv. Mater.* **1998**, *10*, 1519. (d) Fernández-Acebes, A.; Lehn, J. M. *Chem.—Eur. J.* **1999**, *5*, 3285. (e) Chen, B. Z.; Wang, M. Z.; Wu, Y. Q.; Tian, H. *Chem. Commun.* **2002**, 1060. (f) Tian, H.; Chen, B. Z.; Tu, H.; Mullen, K. *Adv. Mater.* **2002**, *14*, 918. (g) Jukes, R. T. F.; Adamo, V.; Hartl, F.; Belser, P.; De Cola, L. *Inorg. Chem.* **2004**, *43*, 2779. (h) Konaka, H.; Wu, L. P.; Munakata, M.; Kuroda-Sowa, T.; Maekawa, M.; Suenaga, Y. *Inorg. Chem.* **2003**, *42*, 1928. (i) Qin, B.; Yao, R. X.; Tian, H. *Inorg. Chim. Acta* **2004**, *357*, 3382. (j) Sud, D.; McDonald, R.; Branda, N. R. *Inorg. Chem.* **2005**, *44*, 5960. (k) Jung, I.; Choi, H. B.; Kim, E. Y.; Lee, C. H.; Kang, S. O.; Ko, J. J. *Tetrahedron* **2005**, *61*, 12256. (l) Uchida, K.; Inagaki, A.; Akita, M. *Organometallics* **2007**, *26*, 5030. (m) Lemieux, V.; Spantulescu, M. D.; Baldridge, K. K.; Branda, N. R. *Angew. Chem., Int. Ed.* **2008**, *47*, 5034. (n) Roberts, M. N.; Carling, C.-J.; Nagle, J. K.; Branda, N. R.; Wolf, M. O. *J. Am. Chem. Soc.* **2009**, *131*, 16644.

(6) (a) Yam, V. W.-W.; Ko, C.-C.; Zhu, N. *J. Am. Chem. Soc.* **2004**, *126*, 12734. (b) Ko, C.-C.; Kwok, W.-M.; Yam, V. W.-W.; Phillips, D. L. *Chem.—Eur. J.* **2006**, *12*, 5840. (c) Ko, C.-C.; Lam, W. H.; Yam, V. W.-W. *Chem. Commun.* **2008**, 5203. (d) Yam, V. W.-W.; Lee, J. K.-W.; Ko, C.-C.; Zhu, N. *J. Am. Chem. Soc.* **2009**, *131*, 912. (e) Wong, H.-L.; Ko, C.-C.; Lam, W. H.; Zhu, N.; Yam, V. W.-W. *Chem.—Eur. J.* **2009**, *15*, 10005. (f) Ko, C.-C.; Yam, V. W.-W. *J. Mater. Chem.* **2010**, *20*, 2063. (g) Lee, J. K.-W.; Ko, C.-C.; Wong, K. M.-C.; Zhu, N.; Yam, V. W.-W. *Organometallics* **2007**, *26*, 12. (h) Ngan, T.-W.; Ko, C.-C.; Zhu, N.; Yam, V. W.-W. *Inorg. Chem.* **2007**, *46*, 1144. (i) Poon, C.-T.; Lam, W. H.; Wong, H.-L.; Yam, V. W.-W. *J. Am. Chem. Soc.* **2010**, *132*, 13992. (j) Wong, H.-L.; Tao, C.-H; Zhu, N.; Yam, V. W.-W. *Inorg. Chem.* **2011**, *50*, 471. (k) Duan, G.; Yam, V. W.-W. *Chem.—Eur. J.* **2010**, *16*, 12642. (l) Duan, G.; Zhu, N.;

Yam, V. W.-W. *Chem.—Eur. J.* **2010**, *16*, 13199. (m) Lee, P. H.-M.; Ko, C.-C.; Yam, V. W.-W.; Zhu, N. *J. Am. Chem. Soc.* **2007**, *129*, 6058.

(7) (a) Ko, C.-C.; Wu, L. X.; Wong, K. M.-C.; Zhu, N. Y.; Yam, V. W.-W. *Chem.—Eur. J.* **2004**, *10*, 766. (b) Querol, M.; Bozic, B.; Salluce, N.; Belser, P. *Polyhedron* **2003**, *22*, 655. (c) Bahr, J. L.; Kodis, G.; Garza, L.; Lin, S.; Moore, A. L.; Moore, T. A.; Gust, D. *J. Am. Chem. Soc.* **2001**, *123*, 7124. (d) Yam, V. W.-W.; Ko, C.-C.; Wu, L. X.; Wong, K. M.-C.; Cheung, K.-K. *Organometallics* **2000**, *19*, 1820. (e) Khairutdinov, R. F.; Giertz, K.; Hurst, J. K.; Voloshina, E. N.; Voloshin, N. A.; Minkin, V. I. *J. Am. Chem. Soc.* **1998**, *120*, 12707.

(8) Williams, J. A. G. *Top. Curr. Chem.* **2007**, *281*, 205.

(9) (a) Rausch, A. F.; Thompson, M. E.; Yersin, H. *Chem. Phys. Lett.* **2009**, *468*, 46. (b) Wong, W.-Y.; He, Z.; So, S.-K.; Tong, K.-L.; Lin, Z. *Organometallics* **2005**, *24*, 4079. (c) Zhou, G.-J.; Wang, X.-Z.; Wong, W.-Y.; Yu, X.-M.; Kwok, H.-S.; Lin, Z. *J. Organomet. Chem.* **2007**, *692*, 3461. (d) Zhou, G.-J.; Wang, Q.; Wong, W.-Y.; Ma, D.; Wong, L.; Lin, Z. *J. Mater. Chem.* **2009**, *19*, 1872. (e) Brooks, J.; Babayan, Y.; Lamansky, S.; Djurovich, P. I.; Tsyba, I.; Bau, R.; Thompson, M. E. *Inorg. Chem.* **2002**, *41*, 3055. (f) Velusamy, M.; Chen., C.-H.; Wen., Y. S.; Lin, J. T.; Lin, C.-C.; Lai, C.-H.; Chou, P.-T. *Organometallics* **2010**, *29*, 3912.

(10) (a) Baldo, M. A.; Lamansky, S.; Burrows, P. E.; Thompson, M. E.; Forrest, S. R. *Appl. Phys. Lett.* **1999**, *75*, 4. (b) Adachi, C.; Baldo, M. A.; Forrest, S. R.; Thompson, M. E. *Appl. Phys. Lett.* **2000**, *77*, 904. (c) Ikai, M.; Tokito, S.; Sakamoto, Y.; Suzuki, T.; Taga, Y. *Appl. Phys. Lett.* **2001**, *79*, 156.

(11) Tan, W.; Zhang, Q.; Tian., H. *Org. Lett.* **2009**, *11*, 161.

(12) Boller, T. M.; Murphy, J. M.; Hapke, M.; Ishiyama, T.; Miyaura, N.; Hartwig., J. F. *J. Am. Chem. Soc.* **2005**, *127*, 14263.

(13) Miyaura., N.; Suzuki., A. *Chem. Rev.* **1995**, *95*, 2457.

(14) Breu, J.; Range, K.-J.; Zelewsky, A.; Yersin, H. *Acta Crystallogr.* **1997**, *53*, 562.

(15) (a) Stückl, A. C.; Klement, U.; Range, K.-J. Z. *Kristallografiya* **1993**, *208*, 297. (b) Giordano, T. J.; Rasmussen, P. G. *Inorg. Chem.* **1975**, *14*, 1628. (c) Ghedini, M.; Pucci, D.; Crispini, A.; Barberio, G. *Organometallics* **1999**, *18*, 2116. (d) Katoh, H.; Miki, K.; Kai, Y.; Tanaka, N.; Kasai, N. *Bull. Chem. Soc. Jpn.* **1981**, *54*, 611.

(16) (a) Ma, B.; Li, J.; Djurovich, P. I.; Yousufuddin, M.; Bau, R.; Thompson, M. E. *J. Am. Chem. Soc.* **2005**, *127*, 28. (b) Chassot, L.; Muller, E.; Von Zelewsky, A. *Inorg. Chem.* **1984**, *23*, 4249.

(17) (a) Fischer, T.; Czerwieniec, R.; Hofbeck, T.; Osminina, M. M.; Yersin, H. *Chem. Phys. Lett.* **2010**, *486*, 53. (b) Kozhevnikov, D. N.; Kozhevnikov, V. N.; Ustinova, M. M.; Santoro, A.; Bruce, D. W.; Koenig, B.; Czerwieniec, R.; Fischer, T.; Zabel, M.; Yersin, H. *Inorg. Chem.* **2009**, *48*, 4179.

(18) Coulson, D. R. *Inorg. Synth.* **1990**, *28*, 107; Angelici, R. J., Ed.

(19) (a) Demas, J. N.; Crosby, G. A. *J. Phys. Chem.* **1971**, *75*, 991. (b) Van Houten, J.; Watts, R. J. *J. Am. Chem. Soc.* **1976**, *98*, 4853. (c) Caspar, J. V.; Meyer, T. J. *J. Am. Chem. Soc.* **1983**, *105*, 5583.

(20) (a) Hatchard, C. G.; Parker, C. A. *Proc. R. Soc. London, Ser. A* **1956**, *235*, 518. (b) Murov, S. L. *Handbook of Photochemistry*; Marcel Dekker: New York, 1973. (c) Kuhn, H. J.; Braslavsky, S. E.; Schmidt, R. *Pure Appl. Chem.* **2004**, *76*, 2105. (d) Wegner, E. E.; Adamson, A. W. *J. Am. Chem. Soc.* **1966**, *88*, 394.

(21) (a) Gagne, R. R.; Koval, C. A.; Lisensky, G. C. *Inorg. Chem.* **1980**, *19*, 2854. (b) Connelly, N. G.; Geiger, W. E. *Chem. Rev.* **1996**, *96*, 877.

(22) *SAINT+. SAX area detector integration program*, Version 7.34A; Bruker AXS, Inc.: Madison, WI, 2006.

(23) Sheldrick, G. M. *SADABS, Empirical Absorption Correction Program*; University of Göttingen: Göttingen, Germany, 2004.

(24) Sheldrick, G. M. *SHELX97. Programs for Crystal Structure Analysis* , (Release 97−2); University of Goetingen: Germany, 1997.

(25) Frisch, M. J.; et al. *Gaussian 03*, Revision E.01; Gaussian, Inc.: Wallingford CT, 2004 (see Supporting Information for the full author list).

(26) (a) Ernzerhof, M; Scuseria, G. E. *J. Chem. Phys.* **1999**, *110*, 5029. (b) Ernzerhof, M.; Perdew, J. P.; Burke, K. *Int. J. Quantum Chem.* **1997**, *64*, 285.

(27) (a) Stratmann, R. E.; Scuseria, G. E.; Frisch, M. J. *J. Chem. Phys.* **1998**, *109*, 8218. (b) Bauernschmitt, R.; Ahlrichs, R. *Chem. Phys. Lett.* **1996**, *256*, 454. (c) Casida, M. E.; Jamorski, C.; Casida, K. C.; Salahub, D. R. *J. Chem. Phys.* **1998**, *108*, 4439.

(28) (a) Barone, V.; Cossi, M. J. *J. Phys. Chem. A* **1998**, *102*, 1995. (b) Cossi, M.; Rega, N.; Scalmani, G.; Barone, V. *J. Comput. Chem.* **2003**, *24*, 669.

(29) Andrae, D.; Häussermann, U.; Dolg, M.; Stoll, H.; Preuss, H. *Theor. Chim. Acta* **1990**, *77*, 123.

(30) Ehlers, A. W.; Böhme, M.; Dapprich, S.; Gobbi, A.; Höllwarth, A.; Jonas, V.; Köhler, K. F.; Stegmann, R.; Veldkamp, A.; Frenking, G. *Chem. Phys. Lett.* **1993**, *208*, 111.

(31) (a) Hehre, W. J.; Ditchfield, R.; Pople, J. A. *J. Chem. Phys.* **1972**, *56*, 2257. (b) Hariharan, P. C.; Pople, J. A. *Theor. Chim. Acta* **1973**, *28*, 213. (c) Francl, M. M.; Pietro, W. J.; Hehre, W. J.; Binkley, J. S.; Gordon, M. S.; Defrees, D. J.; Pople, J. A. *J. Chem. Phys.* **1982**, *77*, 3654.